

82.

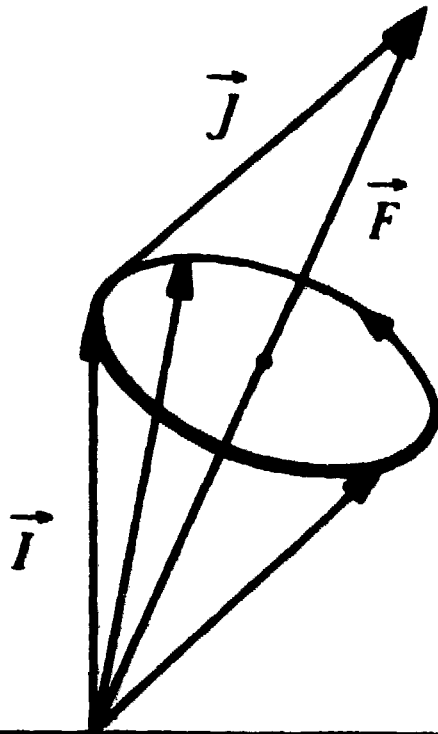
INIS-mf-3098

NL76 E 20 24

**NUCLEAR MAGNETIC MOMENT**

**MEASUREMENTS THROUGH HYPERFINE**

**INTERACTIONS IN HIGHLY STRIPPED IONS**



**ROBERT EDWARD HORSTMAN**

# Stellingen behorende bij het proefschrift

van

R.E. Horstman

## NUCLEAR MAGNETIC MOMENT MEASUREMENTS THROUGH HYPERFINE INTERACTIONS IN HIGHLY STRIPPED IONS

### I

De beschrijving door Goldring et al. van hoekcorrelaties waarbij de deeltjes niet op  $0^\circ$  of  $180^\circ$  gedetecteerd worden is onjuist.

*G. Goldring et al., Phys. Rev. Lett.* 28 (1972) 763.

### II

De uitdrukkingen voor de hoekcorrelaties gegeven door Cramer en Eidson zijn, in tegenstelling tot de in dit proefschrift gegeven beschrijving, niet eenvoudig te corrigeren voor eindige openingshoeken van detectoren en voor relativistische en deoriëntatie effecten.

*J.G. Cramer en W.W. Eidson, Nucl. Phys.* 55 (1964) 593;  
Hoofdstuk I van dit proefschrift.

### III

De door Goldberg et al. gegeven factor  $\kappa$ , waarmee de precessie van de kernspin I in vrije gepolariseerde ionen evenredig zou zijn, is tenminste een factor 2I te groot.

*M.B. Goldberg et al., aangeboden voor publicatie in Phys. Rev. Lett.*

#### IV

De aanname dat de bezetting van aangeslagen electronen-toestanden van vergelijkbare energie statistisch is, is aan twijfel onderhevig.

*F. Beck et al., Proc. Int. Conf. on Hyperfine interactions (Uppland Graviska, Uppsala, 1974), p. 96;*  
*Hoofdstuk I van dit proefschrift.*

#### V

De veronderstelling dat de ladingsverdeling van ionen in vacuüm onafhankelijk is van het doorlopen materiaal is onjuist.

*J.B. Marion en F.C. Young, Nuclear reaction analysis (North-Holland, Amsterdam, 1968);*  
*H.D. Betz, Revs. Mod. Phys. 44 (1972) 465;*  
*Hoofdstuk I van dit proefschrift.*

#### VI

De energiespreiding in een bundel van ionen, met een energie van minder dan enige MeV/nucleon, na het doorlopen van een folie wordt voornamelijk bepaald door fluctuaties in de effectieve lading van het ion tijdens de doorgang door het folie en niet door statistische effecten in de afzonderlijke Coulombinteracties.

*O. Vollmer, Nucl. Instr. 121 (1974) 373;*  
*C. Tschalär, Nucl. Instr. 64 (1968) 273;*  
*R.E. Horstman en M.A. van Driel, intern verslag V3537.*

#### VII

De grootte van de magnetische stootvelden ondervonden door snelle ionen in Fe blijkt niet, zoals Lindhard en Winther berekenen, omgekeerd evenredig met de snelheid te zijn, doch ongeveer evenredig met de snelheid.

*J. Lindhard en A. Winther, Nucl. Phys. A166 (1971) 413;*  
*J.L. Eberhardt et al., publicatie in voorbereiding.*

## VIII

Het experimenteel gevonden verband tussen de elektrische quadrupoolmomenten en de excitatie-energieën van quasi-rotatietoestanden in even-even kernen is in overeenstemming met de beschrijving van deze toestanden in een model met omwentelingssymmetrische romp.

*D.J. Rowe, Nuclear collective motion (Methuen, London, 1970).*

## IX

Het is verwonderlijk dat de waargenomen elektrische quadrupoolovergangen in de Ni-isotopen goed berekend kunnen worden met een model, waarin alleen neutronen buiten een stabiele  $^{56}\text{Ni}$  romp verondersteld worden.

*F.W.M. Glaudemans et al., Nucl. Phys. A198 (1973) 609.*

## X

Met behulp van een Taylor-ontwikkeling naar het aantal neutronen en protonen is in te zien, dat de relatie

$$E_2(Z, N) + E_2(Z+2, N+2) - E_2(Z+2, N) - E_2(Z, N+2) = 0$$

voor de excitatie-energieën van de eerste aangeslagen  $2^+$  toestanden in even-even kernen, uit te breiden is tot iedere kerneigenschap, die binnen het collectieve model als een continue, voldoende langzaam variërende, functie van de massa  $A$  te schrijven is.

*R. Patnaik et al., Phys. Rev. C12 (1975).*

## XI

Het gebruik van atomaire golffuncties, waarin de spin-baan koppelingsterm is meegenomen, is bij het berekenen van hyperfijnstructureffecten een van de beste methoden om deze golffuncties te toetsen.

*L. Armstrong, Theory of hyperfine structure of free atoms (Wiley-Interscience, New York, 1971).*

## XII

Bij de opstelling, die Moi gebruikte om Li-gedrifte Si- en Ge-kristallen te vervaardigen, is de dampdruk van het Li ter plaatse van het kristal niet voorspelbaar.

M.F. Moi, *Electrochem. Techn.* 5 (1967) 551;

R.E. Horstman, *intern verslag V3299*.

## XIII

De belichtingstijd nodig voor het vergroten van een negatief is niet, zoals veelal wordt aangenomen, evenredig met het kwadraat van de lengte van het geprojecteerde beeld, doch evenredig met het kwadraat van de som van de lengten van beeld en voorwerp (negatief).

## XIV

Het uitgeven van steratlassen gebaseerd op het equinoctium van 1975 is weinig zinvol en kan zelfs misleidend zijn voor amateur astronomen, omdat door de Internationale Astronomische Unie (I.A.U.) is afgesproken om in officiële publicaties en in de jaarlijkse handboeken alleen de voor de precessie van de aarde gecorrigeerde equinoctia van de jaren 1900, 1950, 2000 etc. te gebruiken.

## XV

De huidige tendens naar centralisatie van computersystemen zal door de te laag blijvende rekensnelheden weer worden omgebogen naar een decentralisatie.

## XVI

Het is, gezien de huidige inflatie, juister te spreken over inkomensverhoudingen dan over inkomensverschillen.

*NUCLEAR MAGNETIC MOMENT MEASUREMENTS  
THROUGH HYPERFINE INTERACTIONS IN  
HIGHLY STRIPPED IONS*

*PROEFSCHRIFT*

*TER VERKRIJGING VAN DE GRAAD VAN DOCTOR IN  
DE WISKUNDE EN NATUURWETENSCHAPPEN AAN DE  
RIJKSUNIVERSITEIT TE UTRECHT, OP GEZAG VAN  
DE RECTOR MAGNIFICUS PROF. DR. S.J. GROENMAN,  
VOLGENS BESLUIT VAN HET COLLEGE VAN DECANEN  
IN HET OPENBAAR TE VERDEDIGEN OP MAANDAG  
24 NOVEMBER 1975 DES NAMIDDAGS TE 4 15 UUR*

*DOOR*

*ROBERT EDWARD HORSTMAN*

*GEBOREN OP 19 JANUARI 1948 TE SCHIEDAM*

*PROMOTOR*

*PROF. DR. P.M. ENDT*

*DIT PROEFSCHRIFT KWAM TOT STAND ONDER LEIDING VAN*

*DR. G. VAN MIDDELKOOP*

*Onze namen zijn het licht,  
dat 's nachts op de baren  
der zee gloeit en dan uitdooft  
zonder een teken achter te laten.*

*Tagore*



## VOORWOORD

Het gereedkomen van dit proefschrift stelt mij in staat om allen die aan de totstandkoming ervan hebben bijgedragen van harte te bedanken. De verkregen resultaten, beschreven in dit proefschrift, zijn in ruime mate te danken aan de kwaliteit van het werk van vele anderen. Hierbij doel ik in de eerste plaats op de makers van de voor de metingen zo essentiële plunger. Nico van Zwol, Jan Sodaar en Dirk Balke, dit was een mooi stukje werk! Verder wil ik in dit verband J.P. Cooyman bedanken voor het freezezen van de plunger kamer en J.A. Reynders (Groningen) voor het vervaardigen van de voortreffelijke plunger folies. Een aantal trefplaatjes werd gemaakt door Adrie Michielsen. De 6MV tandem Van de Graaff versneller werd gedurende mijn onderzoeksperiode door de technische staf Bram Vermeer, Ben Strasters, Henk Kersemaekers, John van der Fluit en Jaap Jasperse in een steeds betere conditie gebracht, zodat nu zelfs zonder problemen met 7 MV gewerkt kan worden. In geval van machine storingen kon ook tijdens de avonden en weekeinden altijd op hun hulp gerekend worden.

Zonder de door Kees Prins en de electronica ploeg in de loop van de laatste tijd aangebrachte aanzienlijke uitbreiding van het computer systeem, zou de analyse van de metingen bijna onmogelijk zijn geweest. Bovendien hebben Kees Prins en Robert Jan Elsenaar mij vele malen geholpen de computer weer op gang te brengen.

Verder heb ik de hulp, die geboden werd door Leo Wiggers, Pieter Hogenbirk, Henri Aarts, Willie Meijers en Marius Laros bij het experimentele werk en vooral de hulp door Chris Otten bij het meer theoretische werk, zeer op prijs gesteld.

Jaap Koops, Peer Zalm en Jan van Hienen hielden mij op de hoogte van hun schillenmodel berekeningen.

Een betere beheersing van het Engels werd mij bijgebracht door onze Engelse gast Andrew Doubt. Andrew, hierbij wil ik je van harte bedanken voor het werk, waaronder veel correctie werk, dat je de laatste twee jaar voor mij verricht hebt.

Co Eberhardt, jou wil ik graag bedanken voor de vier jaar waarin we zo prettig hebben samengewerkt in vrijwel gelijksoortig onderzoek. Tijdens de vele experimenten en zeilwedstrijden heb ik je als een goede vriend leren kennen.

Ger van Middelkoop, onder jouw leiding en door vele van jouw ideeën is dit proefschrift tot stand gekomen. Ik wil je van harte bedanken voor de bijzonder prettige samenwerking en voor de vele dagen en nachten, die je aan dit onderzoek hebt willen besteden. Ook Judith ben ik dankbaar voor de geboden gastvrijheid tijdens de laatste drukke fase waarin dit proefschrift werd voltooid.

Mijn promotor, Professor Endt, ben ik erkentelijk voor zijn voortdurende interesse in dit onderzoek en voor zijn kritische opmerkingen tijdens de voorbereidingen van dit proefschrift.

Verder wil ik ook mijn ouders bedanken, die mij de gelegenheid boden tot deze studie en die mij ook tijdens mijn promotie onderzoek zeer tot steun waren.

Aan de vormgeving van dit proefschrift hebben Diet Bos, Hilde Elberse en H.M. van Zoest veel bijgedragen. Diet, hartelijk bedankt voor het vele en zorgvuldige typewerk dat je in zo'n korte tijd moest verrichten. De Noord-Hollandse Uitgevers Maatschappij ben ik erkentelijk voor haar toestemming een artikel uit Nuclear Physics te mogen gebruiken voor dit proefschrift.

De mogelijkheid om dit onderzoek te verrichten heb ik te danken aan een plaats, beschikbaar gesteld uit de beleidsruimte van de Stichting voor Fundamenteel Onderzoek der Materie.

---

# CONTENTS

|   |    |
|---|----|
| INTRODUCTION AND SUMMARY  | 1  |
| CHAPTER I. RECOIL-DISTANCE MEASUREMENTS OF g-FACTORS<br>FOR $^{24}\text{Mg}(2_1^+)$ AND $^{20}\text{Ne}(2_1^+)$                     | 6  |
| Abstract  | 6  |
| 1. Introduction   | 6  |
| 2. The experiments  | 7  |
| 2.1. Principle of the measurements  | 7  |
| 2.2. The experimental set-up  | 9  |
| 2.3. Target preparation and mounting  | 10 |
| 2.4. Experimental conditions  | 10 |
| 2.5. Data collection  | 11 |
| 3. Results and interpretation   | 13 |
| 3.1. Data analysis  | 13 |
| 3.2. Electron configurations and fields   | 15 |
| 3.3. The vertical slit  | 17 |
| 3.4. Results  | 21 |
| 3.4.1. The g-factors  | 21 |
| 3.4.2. Error analysis   | 22 |
| 3.4.3. Populations of electronic states   | 24 |
| 3.4.4. The lifetime measurements  | 27 |
| 4. Theoretical discussion and conclusions   | 28 |
| 4.1. Theoretical discussion   | 28 |
| 4.2. Conclusions  | 29 |
| References  | 30 |
| CHAPTER II. RECOIL-DISTANCE MEASUREMENT OF THE g-FACTOR<br>OF $^{22}\text{Ne}(2_1^+)$ AND A TRANSIENT MAGNETIC FIELD<br>CALIBRATION | 32 |
| Abstract  | 32 |
| 1. Introduction   | 32 |
| 2. Description of the experiments   | 33 |
| 2.1. The recoil-distance measurements   | 33 |
| 2.2. The transient field spin-precession measurements   | 36 |
| 2.3. Target preparation   | 39 |

|  |    |
|--|----|
| 3. Results and interpretation                              | 40 |
| 3.1. The recoil-distance measurements                      | 40 |
| 3.2. The transient field measurements                      | 45 |
| 4. Theoretical discussion of the g-factor                  | 48 |
| 5. Conclusions   | 49 |
| References   | 51 |
| <br>   |    |
| CHAPTER III. CONCLUSIONS                                   | 52 |
| <br>   |    |
| 1. The results obtained from the present experiments       | 52 |
| 2. Future experiments within the limitations of the method | 54 |
| 3. Extension to very short lived states                    | 56 |
| References   | 57 |
| <br>   |    |
| SAMENVATTING   | 58 |
| <br>   |    |
| CURRICULUM VITAE   | 60 |

## INTRODUCTION AND SUMMARY

To test theoretical models of the nucleus, which have been developed over the last decades, a large body of experimental data is required. Observable quantities that can be used for these tests are for instance excitation energies, angular momenta (spins) and parities of nuclear states and  $\gamma$ -ray transition probabilities between these states. In a comparison of computed transition probabilities with experimental values one tests the wave functions describing the initial and final states *together*. The wave function of a *single* state can only be tested with electromagnetic properties characteristic for this state, such as the magnetic dipole or the electric quadrupole moment.

This thesis describes some precision measurements of magnetic dipole moments of short-lived nuclear excited states with mean lifetimes of  $\tau = 1-5$  ps. The magnetic moment  $\vec{\mu}$ , which is aligned with the nuclear spin  $\vec{I}$ , is determined from the interaction energy  $W = -\vec{\mu} \cdot \vec{B}$  in a magnetic field  $\vec{B}$ . The interaction leads to a Zeeman splitting of the magnetic substates of the nuclear state. The  $\gamma$ -rays deexciting the various magnetic substates with small and equal energy differences  $\hbar\omega_L = \mu B/\hbar I$  interfere. In a classical picture the nuclear spins precess about the magnetic field direction with a Larmor frequency  $\omega_L = \mu B/\hbar I$ . It is customary to express the magnetic moment  $\vec{\mu}$  as  $\vec{\mu} = g\vec{I}\mu_N$ , where  $\mu_N$  is the nuclear magneton and  $g$  is the dimensionless gyromagnetic ratio.

When the excited state of the nucleus is produced in a nuclear reaction the spin of this state will generally have

a preferred direction. The resulting unequal substate populations (alignment) lead to an anisotropic intensity distribution of the  $\gamma$ -radiation emitted by the excited nuclei.

The precession of the nuclear spin in a magnetic field can then be detected by measuring the rotation of the  $\gamma$ -ray angular distribution. To observe a precession of at least one mrad within a time of 1-5 ps fields of the order of 100 T are needed. The only available magnet at present that can produce a field strong enough is the electron itself provided it is close enough to the nucleus.

Strong fields are for instance obtained during the slowing-down of the excited nucleus in a polarized ferromagnetic material like Fe. The polarized electrons scattered by the Coulomb potential of the moving nucleus cause a magnetic field which is enhanced by a factor of 100 or more over the internal field <sup>1)</sup>. Such measurements are not yet very precise mainly because of the imperfect knowledge of these so-called transient fields.

More precise magnetic moment measurements can be performed by means of the hyperfine interaction in free highly ionized ions. Suppose one has produced a hydrogen-like ion consisting of an excited <sup>24</sup>Mg nucleus with one electron in the 1s orbit. This electron causes an extremely strong magnetic contact field  $B(0)$  at the nucleus. The strength of this field can be calculated exactly and amounts to  $2.89 \times 10^4$  T for <sup>24</sup>Mg. In the free ion the electron spin  $\vec{J}$  couples with the nuclear spin  $\vec{I}$  to a space-fixed vector  $\vec{F}$ . In this example is  $J = \frac{1}{2}$  so that  $F$  can take the values  $I \pm \frac{1}{2}$ . The interference between the states with hyperfine energies  $E_{I+\frac{1}{2}}$  and  $E_{I-\frac{1}{2}}$  is observed as an oscillation with frequency  $\omega = (2I+1)\mu B(0)/\hbar$  in the

$\gamma$ -ray angular distribution. This phenomenon is known as the "quantum beat" <sup>2)</sup>. Hydrogen-like ions can be produced by the stripping of electrons from atoms on passage through a foil at a high recoil velocity obtained in heavy-ion induced reactions. For the investigation of e.g.  $^{24}\text{Mg}$  the  $^{12}\text{C}(^{16}\text{O},\alpha)^{24}\text{Mg}$  reaction was used. A thin carbon target foil was bombarded with high-energy oxygen ions at  $E(^{16}\text{O}) = 37$  MeV (see chapter 1). By detecting the outgoing  $\alpha$ -particles at  $180^\circ$  to the beam direction  $^{24}\text{Mg}$  nuclei in the first-excited  $I^\pi = 2^+$  state were produced with the spins aligned. The  $^{24}\text{Mg}$  ions recoil through the carbon foil into vacuum with a velocity of  $v/c = 0.06$ , where  $c$  is the velocity of light. At this velocity about 15 % of the  $^{24}\text{Mg}$  ions in vacuum is hydrogen-like.

In a classical picture the initially aligned nuclear spins will then, due to the precessions of  $\vec{I}$  and  $\vec{J}$  about  $\vec{F}$ , periodically dealign and align again. Since the electron spins  $\vec{J}$  have no preferred direction this is reflected in periodic attenuations of the  $\gamma$ -ray anisotropy.

The hyperfine-interaction time can be set by a solid stopper (plunger) placed at an adjustable distance behind the target foil. When the ions reach the stopper they will rapidly capture electrons during the slowing-down process. This instantly switches off the hyperfine interaction so that from then on the nuclear spin orientation is frozen. By measuring the  $\gamma$ -ray anisotropy as a function of target-stopper distance one determines the hyperfine frequency  $\omega$ , which is proportional to the magnetic moment. This method was developed by Randolph et al. <sup>3)</sup>.

Not only hydrogen-like ions of  $^{24}\text{Mg}$  are produced on recoil through the carbon target, but also helium-like and

lithium-like ions. Moreover these ions may be in excited states with a strong hyperfine interaction. Although this complicates the measurements it was found that for the cases studied ( $^{20}\text{Ne}$ ,  $^{22}\text{Ne}$  and  $^{24}\text{Mg}$ ) the dominating component came from hydrogen-like ions in the ground state. From a computer fit to the experimental data of intensities of the frequency components for other than ground-state hydrogen-like ions atomic physics information, i.e. the populations of some other electronic states, could be deduced.

Information on these populations for the case of  $^{20}\text{Ne}$  was also obtained from time-integral measurements (i.e. no stopper) in which the different ionic charge states were separated by means of a magnetic spectrograph. The time-integral attenuations of the  $\gamma$ -ray anisotropy for each ionic charge state were measured simultaneously. The results from this measurement show excellent agreement with the plunger data.

If in the one-electron ions the electron spins were polarized a rotation rather than an attenuation of the  $\gamma$ -ray distribution would be observed. An attempt was made to pick up polarized electrons on recoil through a thin magnetized Fe foil. No significant rotation was observed, however, which is probably due to the fact that the polarization is lost by Auger-processes in the ions after they leave the foil. On slowing down in Fe, however, it was found possible <sup>4)</sup> to produce a sizable fraction of ions with a single polarized electron in an s-orbit. Such an experiment has been performed for  $^{22}\text{Ne}$  at an initial ion velocity of  $v/c = 0.05$ . A large rotation (7 mrad) was observed in addition to the transient field precession.

Chapter 1 describes time-differential magnetic moment



measurements on the first-excited  $1^{\pi}=2^{+}$  states in  $^{20}\text{Ne}$  and  $^{24}\text{Mg}$  with mean lives of 1.0 and 2.1 ps, respectively. The lifetime of the latter state was determined simultaneously. A special detection geometry was designed to improve the experimental  $\gamma$ -ray anisotropy measured with finite-size detectors. For  $^{20}\text{Ne}$  also a time-integral measurement with charge-state separation was performed. In this chapter the necessary electronics circuitry built to perform these complicated measurements and the plunger assembly with laser interferometer are also described.

Chapter 2 reports on a magnetic moment measurement of  $^{22}\text{Ne}(2^+)$  with  $\tau = 5.0$  ps and on transient field measurements at low and high recoil velocities.

Some concluding remarks and a discussion of possible extensions of the present techniques are given in chapter 3.

Chapter 1 has been published <sup>5)</sup> and chapter 2 has been accepted for publication <sup>6)</sup>.

#### References

- 1) J. Lindhard and A. Winther, Nucl. Phys. A166 (1971) 413
- 2) H.J. Andr , Physica Scripta 9 (1974) 257
- 3) W.L. Randolph *et al.*, Phys. Lett. 44B (1973) 36
- 4) J.L. Eberhardt, G. van Middelkoop, R.E. Horstman and H.A. Doubt, Phys. Lett. 56B (1975) 329;  
J.L. Eberhardt (Utrecht University), Ph.D. thesis (1975)
- 5) R.E. Horstman *et al.*, Nucl. Phys. A248 (1975) 291
- 6) R.E. Horstman, J.L. Eberhardt, H.A. Doubt and G. van Middelkoop, Nucl. Phys., to be published

# CHAPTER I

## RECOIL-DISTANCE MEASUREMENTS OF $g$ -FACTORS FOR $^{24}\text{Mg}(2_1^+)$ AND $^{20}\text{Ne}(2_1^+)$

**Abstract:** Time-differential recoil-into-vacuum measurements have been performed with a plunger on the first-excited  $1^+ \rightarrow 2^+$  states of  $^{24}\text{Mg}$  and  $^{20}\text{Ne}$ . The states were populated by the reactions  $^{12}\text{C}(^{16}\text{O}, \alpha)^{24}\text{Mg}$  and  $^{12}\text{C}(^{12}\text{C}, \alpha)^{20}\text{Ne}$ . The measured anisotropy of the  $\alpha$ - $\gamma$  angular correlation was greatly increased by means of a vertical slit on the annular particle detector. Values of  $\rho = 0.51 \pm 0.02$  and  $0.54 \pm 0.04$  have been deduced for the  $^{24}\text{Mg}$  and  $^{20}\text{Ne}$   $g$ -factors, respectively. The mean lives of these states have been determined as  $\tau_m = 2.09 \pm 0.13$  ps and  $0.8 \pm 0.2$  ps, respectively. Various theoretical calculations are discussed and compared with the measured  $g$ -factors.

The analysis of the measurement also yields values for the populations of electronic states contributing to the hyperfine interaction. For  $^{20}\text{Ne}$  the populations of the different electronic configurations are compared with the results of a separate time-integral measurement, in which the correlations were measured for each ionic state separately. Large fractions of two-electron excited states are found to contribute.

### 1. Introduction

It has been amply demonstrated that the hyperfine interaction exhibited by single-electron ions affords the possibility of measuring excited-state  $g$ -factors of low- $Z$  nuclei ( $1 \leq Z \leq 8$ ). This hyperfine interaction can be measured time differentially on recoil into vacuum by means of a plunger.

The results of the measurements reported here show that the time-differential method may be extended to excited states with shorter lifetimes (1-2 ps) in nuclei of higher  $Z$  than hitherto. It is also shown that it is possible to use recoil velocities, for which the fraction of single-electron ions is as low as 10-20%, and for which the fractions of two- and three-electron ions thus dominate. Due to the possibility of excitation many electron configurations may then be expected to contribute to the hyperfine interaction. In the present case, however, there are only a few configurations with mean lives longer than the nuclear lifetime which contribute. The interaction energies of these configurations are also quite well known.

The present paper reports the measurement of the  $g$ -factors of the first-excited  $2^+$  states of  $^{24}\text{Mg}$  and  $^{20}\text{Ne}$ . These measurements provide experimental values, with

which the basic theoretical assumptions may be tested and which may also be used in the calibration of other experimental methods, for example, the transient field method<sup>9</sup>). In order to distinguish between various nuclear model calculations of  $g$ -factors of doubly even  $T = 0$  nuclei it is necessary to perform high-precision measurements, since the computed  $g$ -factors are not very different for different configuration spaces and different residual interactions.

For  $^{24}\text{Mg}$  the precision has been considerably improved over an earlier measurement in this laboratory<sup>10</sup>). This was achieved by improving the statistics and the time-of-flight resolution (steps of 1-2  $\mu\text{m}$ ). Moreover, the reliability of the plunger was better determined by continuously monitoring the flatness and position of the target foil with a laser interferometer. It was now possible to follow the oscillation pattern over three periods, compared with little more than one previously. The improved quality of the data leads to a more accurate  $g$ -factor and to an improved sensitivity to the hyperfine interactions of other contributing configurations with more than one electron.

The latter information can be used in the analysis of other more difficult measurements for which either the lifetimes are shorter or for which the percentage of single-electron ions is even lower.

## 2. The experiments

### 2.1. PRINCIPLE OF THE MEASUREMENTS

Single-electron ions can be formed by stripping off electrons at a high recoil velocity on passage through a foil. As an example of the single-electron hyperfine interaction, doubly even nuclei produced in the first-excited  $2^+$  state by heavy-ion reactions with spinless particles [e.g.  $^{12}\text{C}(^{16}\text{O}, \alpha)^{24}\text{Mg}$ ] are discussed in the following.

The detection of outgoing particles close to  $180^\circ$  in an annular detector selects nuclei excited with their spins perpendicular to the beam axis ( $m = 0$  substate population only) and with their momentum directed along this axis (see figs. 1a and 1b). The  $\gamma$ -ray intensity distribution of these selected nuclei has the quadrupole shape shown in fig. 1c at time  $t = 0$ . The magnetic interaction between the excited nucleus and the electron couples the spin  $I$  of the nucleus and the angular momentum  $J$  of the electron to a total angular momentum  $F$  (see fig. 1b). The effects of this static interaction may be qualitatively understood by the following simple considerations.

Classically the vectors  $I$  and  $J$  precess around the space-fixed vector  $F$  with angular frequency  $\omega$ . After half a revolution the nuclear spins are distributed over a sphere, from which two cones along the beam axis are missing (fig. 1b). The shape of the angular distribution of the de-excitation  $\gamma$ -rays at this point, shown in fig. 1c for  $\omega t = \pi$ , resembles the shape generated by nuclei in an  $m = 1$  substate. After a full revolution the spins return to their original positions and the resulting  $\gamma$ -ray distribution again has a quadrupole shape. As a function of time the  $\gamma$ -ray distribution thus shows a breathing mode.

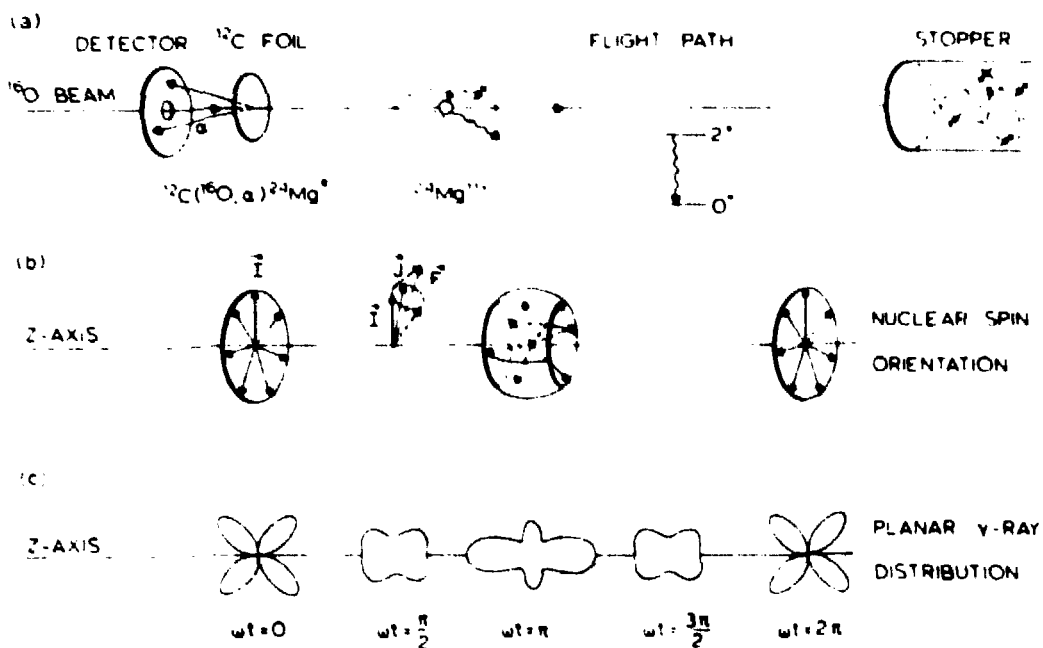


Fig. 1. Simplified classical picture of the nuclear spin deorientation in free ions and its time-differential detection by means of a plunger for the  $^{12}\text{C}(^{16}\text{O}, \alpha)^{24}\text{Mg}$  reaction. Part (a) shows the physical arrangement with a single-electron ion of  $^{24}\text{Mg}(2, ^\circ)$ . Part (b) pictures the hyperfine-interaction coupling of the nuclear spin  $I$  and the electron spin  $J$  to the space-fixed total angular momentum  $F$  and shows the resulting nuclear spin orientation after half a precession revolution ( $\omega t = \pi$ ). Part (c) shows the relevant  $\gamma$ -ray angular distribution patterns at different stages in the deorientation.

Quantum mechanically this phenomenon is described as an interference between states with hyperfine energies  $E_F$  and  $E_{F'}$ , where  $F$  and  $F'$  can take the values  $|I-J|$ ,  $|I-J|+1, \dots, I+J$ . This is known as the "quantum beat"<sup>11)</sup>.

The oscillatory variation in the  $\gamma$ -ray distribution may be sampled by means of a plunger. When the ions reach the stopper the hyperfine interaction is suddenly switched off, due to fast exchange of electrons ( $10^{-16}$  s) followed by the filling of electron orbits during slowing down. At this point the nuclear orientation is frozen in and thus the measured  $\gamma$ -ray distribution from nuclei decaying in the stopper is a function of the target-stopper distance. By variation of this distance the nuclear orientation can be measured time differentially.

From the above discussion and fig. 1c it is plausible that the variation in the  $\gamma$ -ray intensity at  $0^\circ$  or  $90^\circ$  to the beam direction may be written

$$I(t) \propto e^{-t/\tau}(1 - \cos \omega t), \quad (1)$$

where the finite lifetime  $\tau$  of the state is taken into account. The experimental determination of such an oscillatory function enables the frequency  $\omega$ , which is directly related to the nuclear  $g$ -factor, to be deduced. A more rigorous treatment is given in subsect. 3.2.

## 2.2. THE EXPERIMENTAL SET-UP

The first  $2^+$  states of  $^{24}\text{Mg}$  and  $^{20}\text{Ne}$  were excited by means of the heavy-ion reactions  $^{12}\text{C}(^{16}\text{O}, \alpha)^{24}\text{Mg}$  and  $^{12}\text{C}(^{12}\text{C}, \alpha)^{20}\text{Ne}$ . Beams of 41.7 MeV  $^{16}\text{O}^{6+}$  and 36.7 MeV  $^{12}\text{C}^{5+}$  from the Utrecht 7 MV EN tandem accelerator were focussed through a 2 mm diam. Ta diaphragm onto targets consisting of  $500 \mu\text{g}/\text{cm}^2$  Ni,  $300 \mu\text{g}/\text{cm}^2$  Ag and about  $200 \mu\text{g}/\text{cm}^2$  C. The Ni and Ag layers provided good mechanical strength and heat conduction. The foils were stretched over a 4 mm diam stainless steel cylinder. Inside this cylinder the position of a precisely fitting stopper rod was adjusted with a simple screw micrometer. The stability and flatness of the foil were monitored by a He-Ne laser<sup>†</sup> interferometer throughout the experiment. For this purpose the plunger assembly was mounted at an angle of  $30^\circ$  to the beam direction, such that the laser beam could be directed perpendicularly at the beam spot on the target foil (see fig. 2). The distance of closest approach could then be checked whenever desired (subject. 2.4).

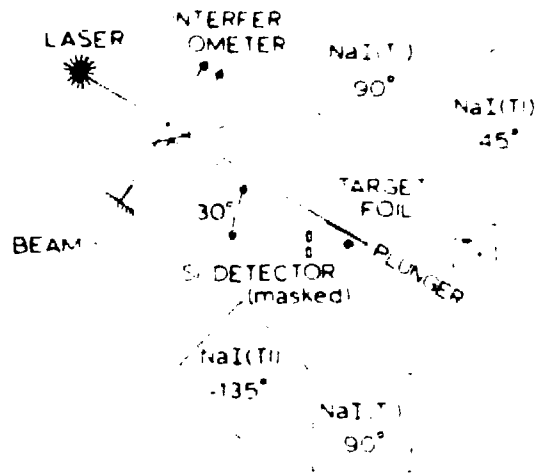


Fig. 2. Schematic horizontal cross section of the experimental set-up showing the  $\alpha$ -particle and  $\gamma$ -ray detectors and the orientation of the plunger to the beam

In the  $^{24}\text{Mg}$  measurement  $\gamma$ -rays were detected coincident with  $\alpha$ -particles in three 12.7 cm diam. by 12.7 cm long NaI(Tl) crystals at angles of  $45^\circ$ ,  $90^\circ$  and  $-90^\circ$  with respect to the beam direction and at a distance of 16 cm from the target. For the  $^{20}\text{Ne}$  measurement a fourth detector was added at  $-135^\circ$  to improve the statistics. A 125 cm<sup>3</sup> Ge(Li) detector was mounted at  $0^\circ$  and at a distance of 11 cm to check the lifetimes of the states.

Outgoing  $\alpha$ -particles were detected in an annular 0.2 mm Si surface-barrier detector, which was masked with a vertical slit to improve the experimental  $\gamma$ -ray anisotropy (see subject. 3.3). The slit subtended angles between  $166.3^\circ$  and  $174.4^\circ$  in the vertical

<sup>†</sup> Manufactured by Spectra Physics, Calif., USA;  $\lambda = 0.6328 \mu\text{m}$ ; 0.5 mW.

plane on either side of the beam and had an opening angle of  $9.8^\circ$  in the horizontal plane.

In the  $^{24}\text{Mg}$  experiment a  $19\ \mu\text{m}$  mylar foil was mounted in front of the detector to stop inelastically backscattered  $^{16}\text{O}$  particles. For  $^{20}\text{Ne}$  the foil was removed, in order to keep the  $\alpha_1$  peak at a higher energy than the  $^{12}\text{C}(^{12}\text{C}, p)$  proton edge.

### 2.3. TARGET PREPARATION AND MOUNTING

The Ni-Ag supporting foils were prepared by vacuum evaporation of Ag followed by electroplating of Ni. A drop of aquadag<sup>†</sup> diluted with alcohol was placed on the foil. After drying at about  $40^\circ\text{C}$  the thickness of the  $^{12}\text{C}$  layer was determined by weighing. Inspection of the target showed that it was reasonably homogeneous and that thickness variations were less than  $1\ \mu\text{m}$ . The target was subsequently mounted on the plunger in dust-free surroundings with the carbon facing the stopper. The measurement was interrupted several times to check that the target remained in good contact with the backing.

The zero distance  $d_0$  of the plunger was measured separately by observation of light shining between the stopper and a precision ruler laid across the cylinder over which the foils were stretched. The zero distance could be measured with a reproducibility of  $1\ \mu\text{m}$  and the values obtained were later shown to be consistent with  $d_0$  obtained from fits to the data. The parallelism of the stopper and the foil were estimated to be within  $1\ \mu\text{m}$  over the whole stopper. It is an advantage of this plunger that no further adjustment is needed.

To obtain the unperturbed angular correlations for Mg and Ne (i.e. the zero-distance points) a  $10\ \text{mg}/\text{cm}^2$  layer of Ag was vacuum evaporated onto the carbon side of the target used in the  $^{24}\text{Mg}$  measurement. The zero-distance points were then measured with the foil remounted in the plunger.

### 2.4. EXPERIMENTAL CONDITIONS

The beam current was maintained at  $100 \pm 20\ \text{nA}$  to avoid excessive heating of the target. This current was chosen as a safe limit by observing the target with the laser interferometer and by requiring that the shift in foil position for beam-on and beam-off remained less than  $0.3\ \mu\text{m}$  ( $\frac{1}{2}$  fringe). This shift was regularly checked and the foil more tightly stretched when necessary, typically once or twice during the experiment. The interferometer was also used to detect the distance of closest approach of the stopper to the foil. This distance was found to be  $6\text{--}8\ \mu\text{m}$  for the three targets discussed here. Contact was probably caused by dust particles pushing against the foil and was found on slowly decreasing the target-stopper separation to the point where the interference pattern changed.

During the measurements a new distance was selected approximately every 40 min. Most points were measured two or three times. For  $^{24}\text{Mg}$  one target was used and

<sup>†</sup> Manufactured by Acheson Colloiden BV, Scheemda, The Netherlands.

the measuring time was 80 h. In the  $^{20}\text{Ne}$  measurement the first target foil deteriorated after 70 h. Both target and stopper were replaced for a second run of 70 h.

After one of the experiments a run was performed with the stopper only and the carbon deposit on the stopper was found to be less than  $5\ \mu\text{g}/\text{cm}^2$ . In spite of good vacuum (an ion-pump mounted directly below the target showed  $2 \times 10^{-6}$  Torr) a thin layer of  $13\ \mu\text{g}/\text{cm}^2$  was deposited on the beam side of the plunger foils (see fig. 4).

## 2.5. DATA COLLECTION

The data collection system is similar to the system briefly described in ref. <sup>12)</sup> Fast timing signals from the  $\alpha$ -particle detector and the  $\gamma$ -ray detectors were used to start and stop the time-to-amplitude converters (TAC). These signals were generated by timing filter amplifiers (TFA) followed by constant fraction timers (CFT), as shown in fig. 3. The output signals of the TAC units were mixed and fed into the "time" analogue-to-digital converter (ADC). Each TAC output was also followed by a single-channel analyzer (SCA), the window of which selected the time range accepted.

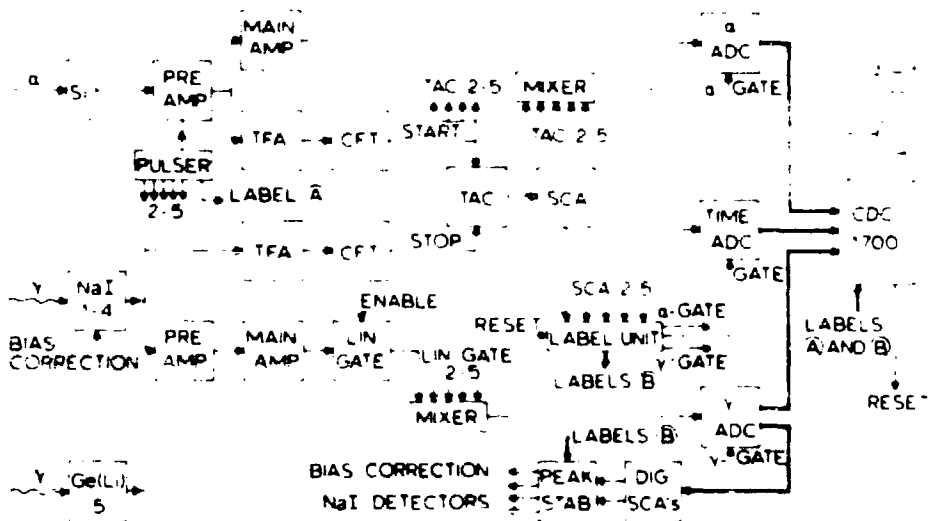


Fig. 3. Scheme of the data collection system. Only one  $\gamma$ -ray detection channel is given in full. The channels for the NaI(Tl) detectors 2-4 and the Ge(Li) detector channel (5) are identical to that of NaI(Tl) detector 1.

The output pulses of the SCA units also served to generate a binary label-bit pattern in the label unit to distinguish different  $\gamma$ -ray detectors and to open linear gates in the analogue channels. The linear gate outputs were mixed and fed into the  $\gamma$ -ADC. The purpose of these gates was to prevent pulse pile-up and cross-talk. The signals from the  $\alpha$ -particle detector after amplification were directly fed into the  $\alpha$ -ADC. The label unit also provided gate pulses for the three ADC units. The digitized  $\alpha$ -particle,  $\gamma$ -ray and time signals were fed into a CDC 1700 computer together with label-bit patterns

defining pairs of coincident detectors. To avoid changes in the labels during conversion the label unit rejected all further pulses until it was reset by the computer.

The experiment was monitored with an on-line sorting procedure, using a disk for spectrum storage, while the raw data were written event by event on magnetic tape for later off-line analysis.

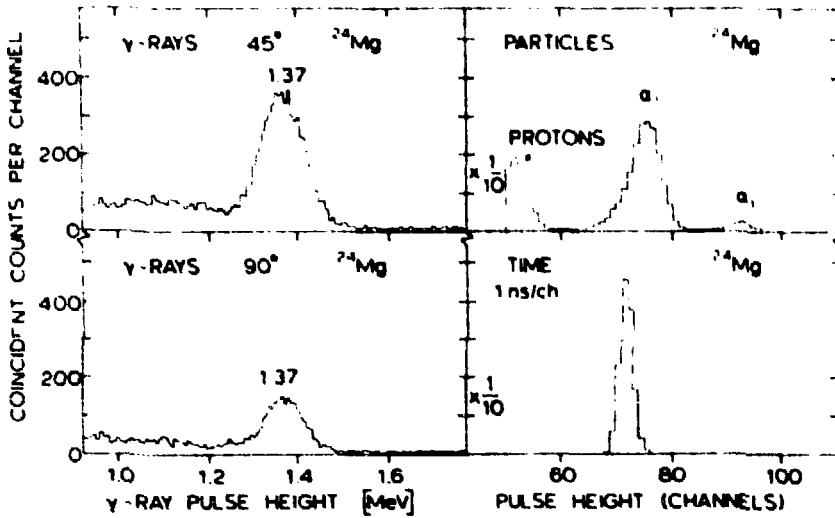


Fig. 4. Coincident  $\gamma$ -ray,  $\alpha$ -particle and time spectra for  $^{24}\text{Mg}$  summed over several runs. For the  $\gamma$ -ray spectra measured at  $45^\circ$  and  $90^\circ$  to the beam direction randoms have been subtracted. Note the  $\alpha_1$  peak due to carbon build-up on the beam side of the target.

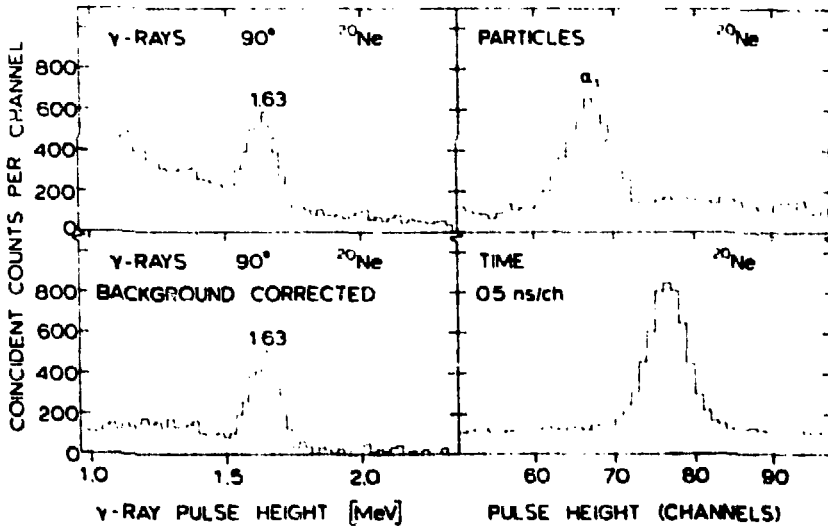


Fig. 5. Coincident  $\gamma$ -ray,  $\alpha$ -particle and time spectra for  $^{20}\text{Ne}$  summed over several runs. The upper random-corrected  $\gamma$ -ray spectrum at  $90^\circ$  to the beam direction is not corrected for coincident background from reactions in the Ni-Ag supporting foil (see the corresponding background in the particle spectrum). The lower  $\gamma$ -ray spectrum is corrected for this coincident background.



Four peak-stabilizers were steered by two labelled digital SCA units set symmetrically about the  $\gamma$ -ray peak in the NaI(Tl) spectra. Gain variations in the photomultipliers were automatically adjusted by small bias corrections and were kept below 2%.

As a check on the electronics a pulser unit sent coincident pairs of pulses to the  $\alpha$ -particle preamplifier and to each of the  $\gamma$ -ray preamplifiers in turn. These test signals were labelled separately to distinguish them from the  $\gamma$ -ray and  $\alpha$ -particle spectra. In this way both the proper functioning of the labelling system and the absence of cross-talk and pile-up could be monitored. Typical  $\alpha$ -particle,  $\gamma$ -ray and time spectra for  $^{24}\text{Mg}$  and  $^{20}\text{Ne}$  are shown in figs. 4 and 5. The time resolution obtained was 4 ns (FWHM).

### 3. Results and interpretation

#### 3.1. DATA ANALYSIS

In the slit geometry it is necessary to measure the  $\gamma$ -ray intensity at  $90^\circ$  for maximum anisotropy (see subsect. 3.3). For reasons of normalization and amplification of the effect the  $\gamma$ -ray intensity at  $45^\circ$  was also measured. Since the stopped and flight fractions are indistinguishable at  $90^\circ$  large NaI(Tl) detectors were used. The ratio  $R(t)$  of coincident  $\gamma$ -ray counts measured at  $90^\circ$  and  $-90^\circ$  to those at  $45^\circ$  and  $-135^\circ$ ,

$$R(t) \equiv \frac{W(90^\circ, t) + W(-90^\circ, t)}{W(45^\circ, t) + W(-135^\circ, t)} \quad (2)$$

behaves as a function of time (target-stopper distance) as a damped oscillation, approximately according to eq. (1) but with the inclusion of the flight fraction, for which the oscillation effects are almost washed out. These ratios  $R$  obtained for  $^{24}\text{Mg}$  and  $^{20}\text{Ne}$  are plotted as a function of target-stopper distance in figs. 6 and 7. To obtain the ratios  $R$  the following corrections have been applied to the contents of the photo-peaks.

The angle-dependent  $\gamma$ -ray absorption in the plunger chamber was determined by replacing the target foil by  $^{60}\text{Co}$  and  $^{88}\text{Y}$  radioactive sources.

All spectra were corrected for random coincidences. This yielded clean spectra for  $^{24}\text{Mg}$  (see fig. 4). For the  $^{20}\text{Ne}$  measurement, however, there remained an appreciable coincident background due to reactions in the Ni backing. This problem did not arise in the  $^{24}\text{Mg}$  experiment because the  $\alpha$ -particle detector was shielded against back-scattered projectiles with a mylar foil (see subsect. 2.2).

To measure this background, a separate run on a bare Ni-Ag foil was performed. The coincident particle spectrum showed a smoothly decreasing slope. Gamma-ray spectra coincident with two windows set at the  $^{20}\text{Ne}$   $\alpha_1$  peak position and at slightly higher energy showed close similarity but differed in intensity by a factor of 1.5. The  $^{20}\text{Ne}$   $\gamma$ -ray spectra were corrected for the coincident background by subtracting 1.5 times the spectrum generated with the off- $\alpha$ -peak window. The effect of this correction is shown in fig. 5.

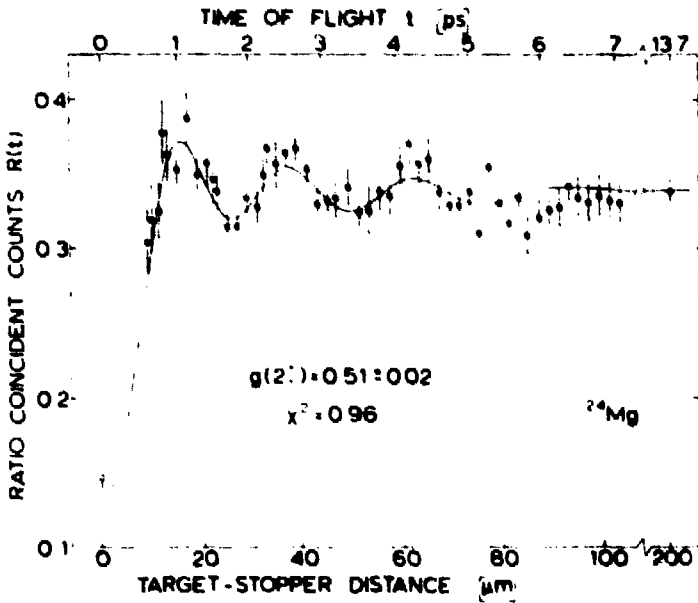


Fig. 6. Ratio of coincident counts  $R(t)$  as a function of perpendicular target-stopper distance for  $^{24}\text{Mg}$ . The curve is a least-squares fit to the data (fit II, see subsect. 3.4.1). The zero-distance point was not used in the fit.

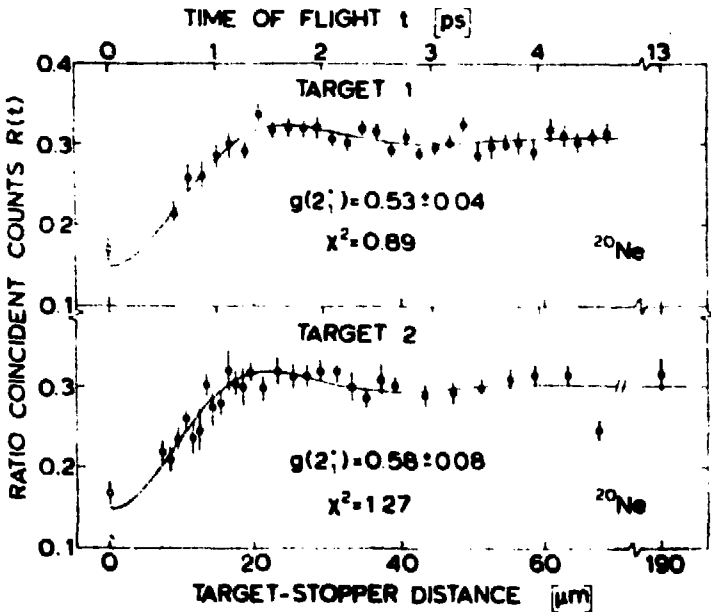


Fig. 7. Ratio of coincident counts  $R(t)$  as a function of perpendicular target-stopper distance for  $^{20}\text{Ne}$  for both targets separately. The curves are least-squares fits to the data (fit I, see subsect. 3.4.1). The zero-distance point was not used in the fits.

No relativistic corrections were necessary because the effect is mainly determined at  $90^\circ$  where these corrections are of second order.

### 3.2. ELECTRON CONFIGURATIONS AND FIELDS

All possible configurations with lifetimes longer than or comparable to the nuclear lifetime and with up to three electrons in the  $1s$ ,  $2s$  and  $2p$  orbits are displayed in table 1. The four-electron configurations have very weak hyperfine interactions or none. Electron configurations with orbits higher than  $2s$  or  $2p$  occupied need not be considered because of Bohr's matching principle<sup>13)</sup>, i.e. electrons with orbital velocities lower than the translational velocity of the moving ion will be stripped off. For  $^{24}\text{Mg}$  and  $^{20}\text{Ne}$  ions emerging from the targets at recoil velocities of  $v/c = 0.06$  charge states with more than four electrons are only weakly populated (less than  $2\%$ ).

TABLE I  
Possible long-lived atomic states for  $n = 1$  and  $n = 2$  in isolated ions

| Configuration              | Term                  | HFI <sup>a)</sup> | $\tau_m(\text{Mg})$            | $\tau_m(\text{Ne})$             |
|----------------------------|-----------------------|-------------------|--------------------------------|---------------------------------|
| <b>Single-electron ion</b> |                       |                   |                                |                                 |
| $(1s)^1$                   | $^2S_{1/2}$           | s                 | $\infty$                       | $\infty$                        |
| $(2s)^1$                   | $^2S_{1/2}$           | w                 | 40 ns <sup>b)</sup>            | 120 ns <sup>b)</sup>            |
| $(2p)^1$                   | $^2P_{1/2, 3/2}$      | w                 | 77 fs <sup>c)</sup>            | 160 fs <sup>c)</sup>            |
| <b>Two-electron ion</b>    |                       |                   |                                |                                 |
| $(1s)^2$                   | $^1S_0$               | n                 | $\infty$                       | $\infty$                        |
| $(1s)^1(2s)^1$             | $^3S_1$               | s                 | 30 ns <sup>b)</sup>            | 110 ns <sup>b)</sup>            |
|                            | $^1S_0$               | n                 | 20 $\mu\text{s}$ <sup>b)</sup> | 130 $\mu\text{s}$ <sup>b)</sup> |
| $(1s)^1(2p)^1$             | $^3P_0$               | n                 |                                |                                 |
|                            | $^3P_1$               | s                 | 20 ps <sup>d)</sup>            | 140 ps <sup>d)</sup>            |
|                            | $^3P_2$               | s                 | 4 ns <sup>b)</sup>             | 5 ns <sup>b)</sup>              |
| <b>Three-electron ion</b>  |                       |                   |                                |                                 |
| $(1s)^2(2s)^1$             | $^2S_{1/2}$           | w                 | $\infty$                       | $\infty$                        |
| $(1s)^2(2p)^1$             | $^2P_{1/2, 3/2}$      | w                 | 1.3 ns <sup>e)</sup>           | 1.8 ns <sup>e)</sup>            |
| $(1s)^1(2s)^1(2p)^1$       | $^4P_{1/2, 3/2, 5/2}$ | s                 | 10 ns <sup>e)</sup>            | 10 ns <sup>e)</sup>             |
| $(1s)^1(2p)^2$             |                       | s                 |                                |                                 |

<sup>a)</sup> Hyperfine interaction (HFI), strong (s), weak (w), null (n).  
<sup>b)</sup> Ref. <sup>39)</sup>. <sup>c)</sup> Ref. <sup>40)</sup>. <sup>d)</sup> Ref. <sup>41)</sup>. <sup>e)</sup> Refs. <sup>23, 24)</sup>.

In the Russel-Saunders  $LS$  coupling scheme the electron spins and the orbital angular momenta couple to  $S$  and  $L$ , respectively, and the total angular momentum is given by  $J = L + S$ . In atomic physics notation such a state is denoted by  $^{2S+1}L_J$ .

Other possible terms not listed in table 1 are Auger unstable or decay by fast X-ray transitions, for which the following selection rules apply:  $\Delta S = 0$  and  $\Delta L = 0, \pm 1$ .

with  $\Delta l = \pm 1$  for the electron causing the transition, and thus  $\Delta J = 0, \pm 1$  but with the exception of  $J = 0 \rightarrow J = 0$ . Excited electron configurations which decay by allowed transitions or, for high excitation energies, by Auger processes have lifetimes of the order of  $10^{-15}$  s, i.e. short compared to the nuclear lifetime. Excited states without the possibility for allowed decay generally have lifetimes long compared to the nuclear lifetime (see table 1) and may contribute to the hyperfine interaction. The main contributions come from configurations with unpaired 1s electrons, which produce high magnetic fields at the nucleus. The states that need to be taken into account in the analysis of the present experiments are listed in table 2, which also includes the total number of components and the highest frequency component for each term relative to that ( $\omega_{1s}$ ) of a single 1s electron.

TABLE 2  
Hyperfine interaction coefficients  $a_j$  used in the analysis of the experiments

| Configuration                            | Term                          | No. of frequencies | $\omega_{\max}/\omega_{1s}$ | $a_j$ (rad · ps <sup>-1</sup> ) |                      |
|--|-------------------------------|--------------------|-----------------------------|---------------------------------|----------------------|
|  |                               |                    |                             | Mg                              | Ne                   |
| <b>Single-electron ion <sup>a)</sup></b> |                               |                    |                             |                                 |                      |
| (1s) <sup>1</sup>                        | <sup>2</sup> S <sub>1/2</sub> | 1                  | 1.00                        | 2.76                            | 1.60                 |
| (2s) <sup>1</sup>                        | <sup>2</sup> S <sub>1/2</sub> | 1                  | 0.125                       | 0.35                            | 0.20                 |
| <b>Two-electron ion</b>                  |                               |                    |                             |                                 |                      |
| (1s) <sup>1</sup> (2s) <sup>1</sup>      | <sup>3</sup> S <sub>1</sub>   | 3                  | 1.11                        | 1.53 <sup>b)</sup>              | 0.89 <sup>b)</sup>   |
| (1s) <sup>1</sup> (2p) <sup>1</sup>      | <sup>3</sup> P <sub>2</sub>   | 9                  | 1.02                        | 0.71 <sup>b)</sup>              | 0.41 <sup>b)</sup>   |
|  | <sup>3</sup> P <sub>1</sub>   | 3                  | 0.52                        | 0.72 <sup>a,c)</sup>            | 0.42 <sup>a,c)</sup> |
| <b>Three-electron ion <sup>d)</sup></b>  |                               |                    |                             |                                 |                      |
| (1s) <sup>2</sup> (2s) <sup>1</sup>      | <sup>2</sup> S <sub>1/2</sub> | 1                  | 0.10                        | 0.28                            | 0.15                 |

<sup>a)</sup> Ref. <sup>13)</sup>.

<sup>b)</sup> Relativistic Hartree-Fock calculation quoted in ref. <sup>21)</sup>.

<sup>c)</sup> Average value of *jj* and *LS* coupling.

<sup>d)</sup> Screening calculated in the alkali approximation with the effective quantum numbers taken from ref. <sup>43)</sup>.

The effect of the hyperfine interaction of an electronic state on the angular correlation as a function of time is given by the attenuation coefficients [eq. (298); ref. <sup>14)</sup>]

$$G_k(t) = \sum_{FF'} C_{FF'} \exp \left\{ -\frac{i}{\hbar} (E_F - E_{F'})t \right\}, \quad (3)$$

where

$$C_{FF'} = (2F+1)(2F'+1) \begin{Bmatrix} F & F' & k \\ 1 & 1 & J \end{Bmatrix}^2 / (2J+1),$$

$$\frac{1}{\hbar} (E_F - E_{F'}) = \omega_{FF'} = \{F(F+1) - F'(F'+1)\} \frac{a_j}{2\hbar} g. \quad (4)$$

The quantities  $\omega_{FF'}$ ,  $g$  and  $a_j$  represent, respectively, the Larmor frequency, the

nuclear  $g$ -factor and the interaction energy defined by Kopfermann <sup>15)</sup> for  $g = 1$ . Eq. (3) is calculated under the assumption of a randomly oriented (i.e. isotropic) hyperfine interaction.

The attenuation coefficients for the sum of the fractions of nuclei decaying in flight and in the stopper are given by

$$G_k(t) = \sum_i \alpha_i \sum_{FF'} C_{FF'} \left\{ e^{-t/\tau} \cos \omega_{FF'}^i t + \frac{1 - e^{-t/\tau} (\cos \omega_{FF'}^i t - \omega_{FF'}^i \tau \sin \omega_{FF'}^i t)}{1 + (\omega_{FF'}^i \tau)^2} \right\}, \quad (5)$$

where  $\alpha_i$  is the population of the  $i$ th electronic state. To illustrate the effect of this function, fig. 8 shows the ratio  $R(t)$  calculated as a function of target-stopper distance for each electronic state given in table 2 separately with a population  $\alpha = 30\%$ . The curve shown for the  $(1s)^1; ^2S_{1/2}$  state, for example, is the measured effect that would be expected in the present  $^{24}\text{Mg}$  experiment, if 30% of the ions were in the single-electron ground state and the rest were distributed between the zero-electron and the ground-state two-electron charge states. The actual fit from fig. 6 is also included for comparison.

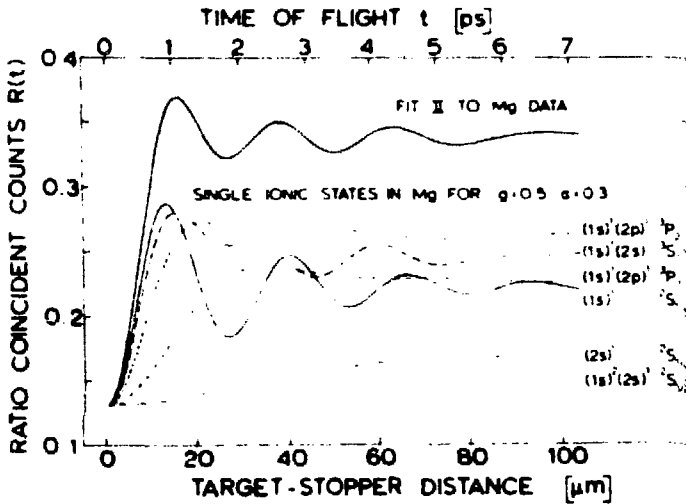


Fig. 8. Ratio of coincident counts  $R(t)$  plotted as a function of the time of flight  $t$  both for fit II to the Mg data (above) and for each ionic state of table 2 separately with a  $g$ -factor  $g = 0.5$  and a population of the state of  $\alpha = 0.3$  (below). The scale below the figure is the perpendicular target-stopper distance.

### 3.3. THE VERTICAL SLIT

In reactions with spinless particles in a collinear geometry, i.e. when the outgoing particles are detected at  $180^\circ$  to the beam direction ( $z$ -axis), the final excited nucleus has only  $m = 0$  magnetic substates populated. Hence the angular correlation of a subsequent  $2^+ \rightarrow 0^+$   $\gamma$ -ray transition shows large anisotropy. Since the particle detector has a finite size, however,  $m = \pm 1$  substates may also be populated, especially

when the incoming particles have high angular momenta [ $l = 6-12$ ; ref. <sup>16</sup>]). In this case an angular correlation with a lower anisotropy will result.

This effect can be clearly demonstrated by the measurement of the direction of the symmetry axis of the correlation for the  $^{12}\text{C}(^{12}\text{C}, \alpha\gamma)^{20}\text{Ne}$  reaction as a function of the angle of  $\alpha$ -detection. For this purpose a position-sensitive detector subtending angles between  $117^\circ$  and  $161^\circ$  with respect to the beam axis was used. The position along the detector was converted to the angle with respect to the beam direction by measuring the position of the  $\alpha$ -radiation shadow cast by a rotatable needle on the position-sensitive detector by an  $^{241}\text{Am}-^{244}\text{Cm}$  source centred in the target chamber. The result of the measurement is displayed in fig. 9. From the fast rotation of the angular correlation symmetry axis with  $\alpha$ -particle detection angle it is obvious that the correlation measured with a relatively large-angle annular detector shows reduced anisotropy.

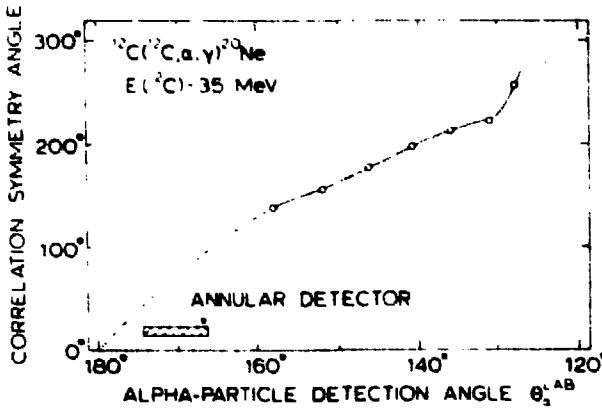


Fig. 9. The  $\gamma$ -ray angular correlation symmetry axis plotted versus the  $\alpha$ -particle detection angle for the  $^{12}\text{C}(^{12}\text{C}, \alpha\gamma)^{20}\text{Ne}$  reaction. The symmetry axis rotates a factor 7.5 faster and in the opposite direction to the  $^{20}\text{Ne}$  recoil direction. For the position of an annular particle detector shown the corresponding  $\gamma$ -ray angular correlation would be attenuated.

For a theoretical description of the  $\gamma$ -ray angular correlation for particles not detected at  $180^\circ$ , it is convenient to choose a new coordinate system, in which the  $x$ -axis is taken along the beam direction and the  $z$ -axis is taken perpendicular to the reaction plane in the direction  $k_1 \times k_0$ , where  $k_1$  and  $k_0$  represent the directions of the incoming heavy and outgoing light particles, respectively. The angular correlation can be written as a function of the azimuthal and polar angles  $\phi$  and  $\theta$ ,

$$W(\theta, \phi) = \sum_{kN} B_k^N(1) G_k(1) A_k(2) Y_k^N(\theta, \phi), \quad (6)$$

with summation over  $k = 0, 2, 4, \dots$  and  $N = -k, -k+2, \dots, +k$ . The  $A_k(2)$  represent the angular correlation coefficients for the transition in the final nucleus and  $Y_k^N(\theta, \phi)$  are spherical harmonics. The coefficients  $B_k^N(1)$  are given by

$$B_k^N(1) = \sum_{mm'} (-1)^m \langle m | \rho^1 | m' \rangle \begin{pmatrix} l & l & k \\ m' & -m & N \end{pmatrix} / \sum_{mm'} (-1)^m \langle m | \rho^1 | m' \rangle \begin{pmatrix} l & l & 0 \\ m' & -m & 0 \end{pmatrix}, \quad (7)$$

where the  $\langle m|\rho^I|m'\rangle$  are the elements of the density matrix of the substates  $m$  after formation of the excited state  $I$  [cf. eq. (33); ref. <sup>14</sup>]. These elements depend on the reaction mechanism and thus must be determined experimentally. In the chosen coordinate system, however, for natural parity states excited in reactions with spinless particles, the Bohr theorem <sup>17</sup>) states that only  $I-m = \text{even}$  substates are populated. Eq. (6) may be derived <sup>9</sup> from eq. (207) in ref. <sup>14</sup>). For a  $2^+ \rightarrow 0^+$  transition in the final nucleus  $W(\theta, \phi)$  becomes proportional <sup>18</sup>) to  $\sin^2\theta$ .

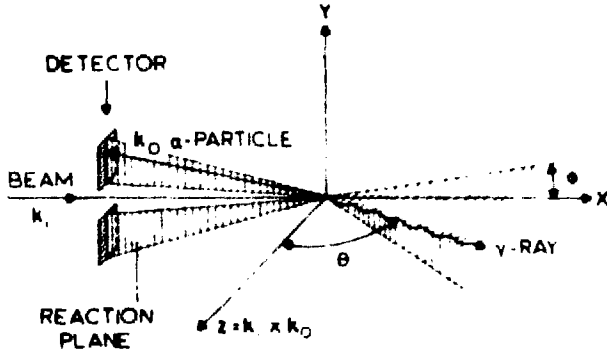


Fig. 10. The slit geometry characterized by a vertical reaction plane defined by the beam direction ( $k_i$ ) and the detected outgoing  $\alpha$ -particle ( $k_o$ ). The horizontal  $z$ -axis is perpendicular to the beam direction. The azimuthal angle  $\phi$  in the  $(x, y)$  plane and the polar angle  $\theta$  with respect to the  $z$ -axis are also indicated.

This proportionality means that for point detectors the correlation function drops to zero along the  $z$ -axis. If the particles are detected not in a point but along a vertical line through the beam axis (see fig. 10), the reaction plane is fixed vertically and the  $z$ -axis is fixed in the horizontal plane at  $90^\circ$  to the beam direction ( $\theta = 0^\circ$ ). Thus in the case of a vertical mask on the annular detector a maximum anisotropy for the unperturbed correlation will be obtained. The density matrix elements, however, also depend on the detection angle of the  $\alpha$ -particles. On averaging over the detection

<sup>9</sup> The density matrix in eq. (7), which has a simple form for the present coordinate system and reaction [four unknown parameters <sup>18</sup>)], is transformed to a system with arbitrary  $z'$  axis (for example in the direction of an external magnetic field) as

$$\begin{aligned} \langle \mu|\rho^I|\mu'\rangle &= \sum_{mm'} \langle m|\rho^I|m'\rangle D_{m'\mu}^J(z \rightarrow z') D_{m\mu}^{J*}(z \rightarrow z') \\ &= \sum_{k\tau N} B_k^N \begin{pmatrix} I & I & k \\ \mu' & -\mu & \tau \end{pmatrix} D_{-\mu-\mu, -\tau}^k(z \rightarrow z') \end{aligned}$$

where  $D_{m'\mu}^J(z \rightarrow z')$  is an element of the matrix that carries out a rotation of the quantization system  $z$  into a system  $z'$  [eq. (9); ref. <sup>14</sup>]. This density matrix replaces the density matrix  $\langle m|\rho(k_i)|m'\rangle$  in eq. (207) of ref. <sup>14</sup>). Eq. (6) can now be derived with eqs. (208), (209) and (298) in ref. <sup>14</sup>).

angle and using the Bohr theorem eq. (6) can be rewritten as

$$\begin{aligned}
 W(\theta, \phi) = & Y_0^0 + A_2 Q_2 G_2(\tau) [B_2^0 Y_2^0(\theta, \phi) + 2B_2^2 \operatorname{Re} \{Y_2^2(\theta, \phi)\}] \\
 & + A_4 Q_4 G_4(\tau) \left[ \left( \frac{1}{12} \sqrt{14 - \frac{3}{2} B_2^0} \right) Y_4^0(\theta, \phi) + \frac{1}{3} \sqrt{15} B_2^2 \operatorname{Re} \{Y_4^2(\theta, \phi)\} \right. \\
 & \left. + 2B_4^4 \operatorname{Re} \{Y_4^4(\theta, \phi)\} \right]. \quad (8)
 \end{aligned}$$

where the geometrical attenuation coefficients  $Q_k$  have been introduced [see ref. <sup>14</sup>, p. 1691]. Note that the averaged coefficients  $B_3^0$  and  $B_4^2$  do not appear in eq. (8), since they are related to the coefficients  $B_2^0$  and  $B_2^2$ . For symmetry reasons the coefficients  $B_0^2$ ,  $B_2^2$  and  $B_4^2$  are real and may be determined experimentally. This was carried out with the zero-distance-point target (see subject. 2.3) in separate unperturbed angular correlation measurements, in which the slit was taken successively at 0°, 45° and 90° to the  $\gamma$ -ray detector plane. In this way the correlations were measured three-dimensionally. The result of the measurement for  $^{20}\text{Ne}$  is displayed in fig. 11.

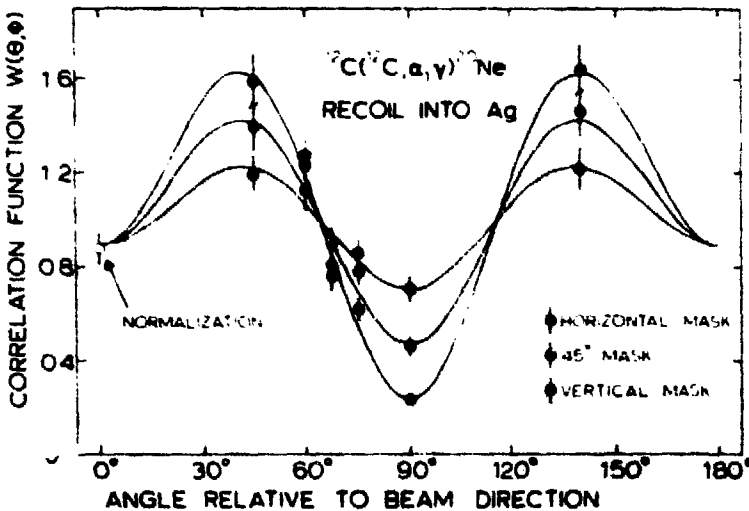


Fig. 11. Alpha-gamma angular correlations with the  $^{20}\text{Ne}$  reaction measured for the three orientations of the rectangular mask. The three curves were fitted simultaneously to the experimental points normalized to the coincident yield at 0°.

The figure clearly shows that the minimum anisotropy is found, as expected, for the horizontal slit, for which the  $z$ -axis is perpendicular to the horizontal  $\gamma$ -ray plane. The correlation measured for the 45° slit corresponds roughly to the correlation measured for the unmasked detector. The  $B_k^N$  parameters, extracted by a simultaneous fit to the three correlations with allowance for the finite width of the slit, were used in the subsequent analysis of the plunger data.



### 3.4. RESULTS

*3.4.1. The g-factors.* The corrected data from the  $^{24}\text{Mg}$  and both  $^{20}\text{Ne}$  measurements (see subsect. 3.1) are shown in figs. 6 and 7. The perpendicular target-stopper distances are given below the figures, whereas above the figures the actual time of flight of the ions from the target to the stopper along the beam axis is given.

A computer program was written to perform a non-linear least-squares fit of the function  $R(t)$  for the electronic states of table 2 to the data points, taking into account the finite width of the slit. An uncertainty of  $1\ \mu\text{m}$  in the setting of the micrometer was also assumed.

Three types of fit (I-III) were performed for  $^{24}\text{Mg}$ . In the first the populations of the  $^3\text{S}_1$ ,  $^3\text{P}_2$  and  $^3\text{P}_1$  states, which have about the same excitation energy, were assumed to be statistically distributed with weights  $2J+1$ . The other free parameters in the fit were the population of the single-electron ground state, the  $g$ -factor and the zero distance of the plunger i.e. four free parameters in total and 53 experimental points. In the second type of fit the populations of the  $^3\text{S}_1$  state and of the two  $^3\text{P}$  states taken together were allowed to vary independently. In the third type the populations of all three triplet states were allowed to vary independently. The result of fit II is shown in fig. 6. For  $^{20}\text{Ne}$  only the first type of fit, with the smallest number of free parameters, was stable and was used for both targets (in each case 31 experimental points, see fig. 7).

For completeness small, fixed contributions from the single-electron excited state and the three-electron ground state, which have small interaction coefficients (see table 2 and fig. 8), were included in the fits. The effect on the fitted parameters was negligible, but the value of  $\chi^2$  became marginally worse. For  $^{20}\text{Ne}$  the amounts of these contributions were taken from a separate integral measurement involving charge-state separation in a magnetic spectrograph (see subsect. 3.4.3). For  $^{24}\text{Mg}$  the amplitudes of the two contributions were fitted separately to the data. This gave upper limits for the populations  $\alpha[(2s)^1]$  and  $\alpha[(1s)^2(2s)^1]$  of 0.08 and 0.11, respectively, at the three standard deviation limit. The latter limit is rather lower than the population expected from the three-electron fraction. A value of 0.10 has been used in the analysis (see table 4).

The  $g$ -factors extracted from the fits for  $^{24}\text{Mg}$  and  $^{20}\text{Ne}$  are displayed at the bottom of table 3. This table also details the separate contributions (treated independently) to the final quoted errors of 4 % and 8 %, respectively. The values of the populations  $\alpha$  extracted for the various electronic states for the different types of fit are given in table 4 and are discussed in subsect. 3.4.3.

The value of the  $g$ -factor for  $^{24}\text{Mg}$  did not depend very strongly on the type of fit performed i.e. on the relative populations of the excited two-electron states. Fits II and III gave almost identical results i.e. no new information was obtained from the six-parameter fit. Fit I gave a value that was 2.8 % higher than fit II and the fit was somewhat poorer with a  $\chi^2$  value of 1.1 compared to 1.0. The value of the  $g$ -factor quoted in table 3 is the average of the values obtained for fits I and II. The spread of

TABLE 3  
Error analysis and final results for the  $g$ -factors

| Source of error       | Contribution to error (%)     |                                    |                               |
|-----------------------|-------------------------------|------------------------------------|-------------------------------|
|                       | $^{24}\text{Mg}(2, ^\circ)$   | $^{20}\text{Ne}(2, ^\circ)$        |                               |
|                       |                               | target 1                           | target 2                      |
| Statistics            | 2.1                           | 6.3                                | 7.9                           |
| Zero distance         | 1.7                           | 3.3                                | 8.8                           |
| Target thickness      | 2.3                           | 2.3                                | 2.3                           |
| Lifetime              | 0.2                           | 2.4                                | 3.9                           |
| Two-electron analysis | 1.4                           | 1.4 <sup>a)</sup>                  | 1.4 <sup>a)</sup>             |
| $a_J(^3\text{S}_1)$   | 0.6                           | 0.6 <sup>a)</sup>                  | 0.6 <sup>a)</sup>             |
| $a_J(^3\text{P}_1)$   | 0.3                           | 0.3 <sup>a)</sup>                  | 0.3 <sup>a)</sup>             |
| Coincident background | 0.0                           | 2.0                                | 6.0                           |
| Total error           | 3.9                           | 8.2                                | 14.1                          |
| $g$ -factor $g$       | $0.51 \pm 0.02$ <sup>b)</sup> | $0.53 \pm 0.04$ <sup>c)</sup>      | $0.58 \pm 0.08$ <sup>c)</sup> |
|                       |                               | mean $0.54 \pm 0.04$ <sup>c)</sup> |                               |

<sup>a)</sup> From the  $^{24}\text{Mg}$  analysis.

<sup>b)</sup> Average of the values obtained for fits I and II.

<sup>c)</sup> Fit I.

1.4% in the  $g$ -factor has been taken to represent the uncertainty in the two-electron analysis (table 3). For  $^{20}\text{Ne}$  this is probably an overestimate, since more ions are in the  $(1s)^1$  state.

The uncertainties in the  $\overline{B}_k^N$  coefficients and the absorption correction introduce negligible errors in the  $g$ -factor. The other sources of error are discussed in the following subsection.

The values of the function  $R(t)$  for  $^{24}\text{Mg}$  and  $^{20}\text{Ne}$  at zero distance were completely determined by the measurements of the  $\overline{B}_k^N$  coefficients (subsect. 3.3). The zero-distance points measured with the plunger (see subsect. 2.3) are shown in figs. 6 and 7 for illustration but were not included in the fits. The zero-distance point for  $^{24}\text{Mg}$ , unlike the rest of the  $^{24}\text{Mg}$  data for which the anisotropy was lower, had to be corrected for coincident background at  $90^\circ$ . The zero-distance points show reasonable agreement with the result of the measurement of the full correlation, although for these two points the background correction may be slightly underestimated.

#### 3.4.2. Error analysis (see also table 3).

(i) *Zero distance.* Values for the zero distances  $d_0$  were derived from the fits for the three experiments with an uncertainty of about  $1 \mu\text{m}$ . The values measured by eye in the manner discussed in subsect. 2.3 were about  $2 \mu\text{m}$  nearer the stopper. The value derived from the  $^{24}\text{Mg}$  lifetime measurement coincided with the result of the measurement by eye. This is good agreement within the errors. A weighted mean of these four values was taken for  $d_0$  for the  $^{24}\text{Mg}$  target and the first  $^{20}\text{Ne}$  target since

these were measured with the same stopper. A mean of the value from the  $g$ -factor fit and the measurement by eye were taken for the second  $^{20}\text{Ne}$  target.

Effects caused by the fast decay of higher-lying electronic states within the nuclear lifetime would give an apparent shift of the zero distance towards the stopper [see for example the treatment of Bosch and Speiser<sup>19</sup>]. The present measurements indicate an upper limit of 150 fs for the possible delay in the switching-on of the hyperfine interaction in Mg and Ne ions.

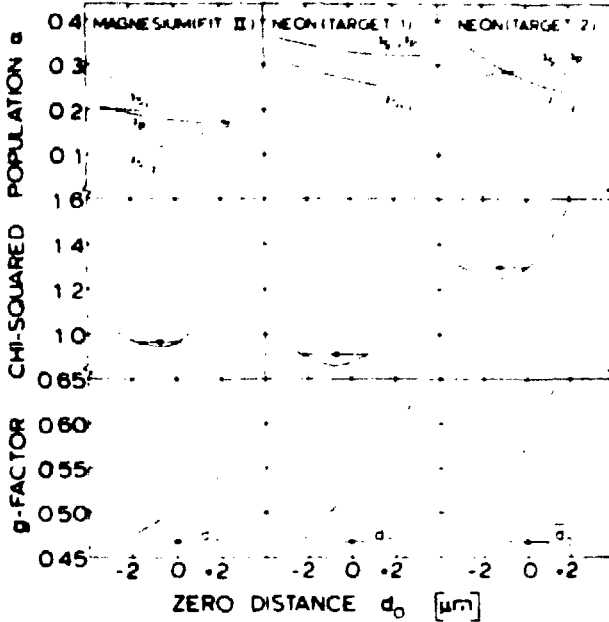


Fig. 12. The dependence of the  $g$ -factor,  $\chi^2$  and the populations  $\alpha$  of the ionic states on the zero distance  $d_0$  of the plunger. The averaged values of  $d_0$  (see subsect. 3.4.2) have been normalized to  $d_0 = 0$  and the uncertainties are indicated. The  $d_0$  values with the errors obtained from the fits are indicated in the  $\chi^2$  plots.

The dependence of the  $g$ -factor on the zero distance  $d_0$  for the three targets is plotted in fig. 12, which also includes the dependence of  $\chi^2$  and of  $\alpha(1s)$  and  $\alpha(^3S + ^3P)$ . These plots demonstrate the confidence with which  $d_0$  may be fitted and also suggest that previous experimenters may have underestimated the importance of this source of error.

(ii) *Target thickness.* The recoil velocities of the  $^{24}\text{Mg}$  and  $^{20}\text{Ne}$  ions were calculated from the kinematics taking into account the thickness of the Ni-Ag supporting foil, the thickness of the  $^{12}\text{C}$  target, the angle of the target with respect to the beam and the opening angle of the  $\alpha$ -particle detector. The values obtained for  $v/c$  were  $(5.58 \pm 0.13)\%$  and  $(5.69 \pm 0.13)\%$ , respectively. The main uncertainty in the velocities stems from the uncertainty in the thickness of the carbon layer. An uncertainty of 50% was assumed in the thickness of  $200 \mu\text{g}/\text{cm}^2$  measured by weighing, to allow for possibly uneven deposit of carbon during drying (see subsect. 2.3).

(iii) *Lifetimes.* The values  $2.09 \pm 0.13$  ps and  $1.04 \pm 0.07$  ps were taken for the lifetimes of the first  $2^+$  states in  $^{24}\text{Mg}$  and  $^{20}\text{Ne}$ , respectively. For  $^{24}\text{Mg}$  the value is that of the present work (subsect. 3.4.4). The error in the lifetime hardly contributes to the error in the  $g$ -factor for  $^{24}\text{Mg}$  (table 3). On treating the lifetime of  $^{24}\text{Mg}$  as a free parameter in the  $g$ -factor fit with  $d_0$  already determined, a consistent value of  $2.1 \pm 0.4$  ps was found.

For the  $^{20}\text{Ne}$  measurement, however, for which the oscillation is quickly damped out by the short lifetime, the  $g$ -factor is more sensitive to the error in the lifetime. From the  $g$ -factor fit values of  $\tau = 1.0 \pm 0.3$  ps and  $0.7 \pm 0.2$  ps were found for the two targets. The average value of  $0.8 \pm 0.2$  ps is in good agreement with the above value used in the analysis, which is a weighted mean quoted in ref. <sup>20)</sup> of two DSA measurements and one Coulomb excitation measurement.

(iv) *Hyperfine interaction coefficients  $a_j$ .* For the  $^3\text{S}_1$  and the  $^3\text{P}_1$  states these coefficients are not exactly known. The  $a_j(^3\text{S}_1)$  coefficients used in the analysis (table 2) were taken from a relativistic Hartree-Fock calculation quoted in ref. <sup>21)</sup>. Calculations of screening with the alkali approximation <sup>15)</sup> give values within 1 % of the Hartree-Fock value assuming that only the 2s electron is screened. The contribution to the error in the  $g$ -factor for  $^{24}\text{Mg}$  (table 3) was obtained assuming an uncertainty in  $a_j(^3\text{S}_1)$  of 3 %.

For the  $^3\text{P}$  states the effects of screening are about 2 % and may be calculated with the alkali approximation. Different values of  $a_j(^3\text{P}_1)$  are obtained for  $jj$  and  $LS$  coupling. Since it is not certain which coupling scheme applies for highly stripped ions, the average of the two values was used in the analysis of the data and the 8 % spread about this value was taken as the uncertainty. The contribution to the error in the  $g$ -factor for  $^{24}\text{Mg}$  was small.

The contributions were taken to be the same for  $^{20}\text{Ne}$  as for  $^{24}\text{Mg}$ . This is a conservative assumption.

(v) *Coincident background.* For the  $^{20}\text{Ne}$  measurements an extra error was introduced to allow for the uncertainty in the coincident background correction factor (see subsect. 3.1).

**3.4.3. Populations of electronic states.** Populations of the electronic states were deduced from the  $g$ -factor fits. The results for the different fits are displayed in table 4. The errors were calculated by taking into account the sources of error discussed in subsect. 3.4.2. The results of fits II and III for the populations of the  $^3\text{S}_1$ ,  $^3\text{P}_2$  and  $^3\text{P}_1$  states in  $^{24}\text{Mg}$  differ significantly from the relative statistical distributions taken for fit I. For another example of a deviation from the statistical distribution, see ref. <sup>22)</sup>. The total population of the excited two-electron state, however, is the same for all three fits within the errors. From fig. 8 it is clear that it is difficult to determine the populations of the  $^3\text{P}_2$  and  $^3\text{P}_1$  states separately in fit III, because these states show such a similar structure.

Confirmation of the existence of a large population in the two-electron excited state of  $^{20}\text{Ne}$  was given by the results of a time-integral measurement, in which the

TABLE 4  
Measured populations of electronic states

| Nucleus                             | Charge state | Fraction of total (%) <sup>a)</sup> | Configuration   | Term                                | Population $\alpha$ of state (%)<br>Plunger measurement <sup>b)</sup> |                        |                        |          |          |
|-------------------------------------|--------------|-------------------------------------|---|-------------------------------------|---|------------------------|------------------------|----------|----------|
|                                     |              |                                     |   |                                     | fit I   | fit II                 | fit III                |          |          |
| <sup>24</sup> Mg                    | 12           | 2                                   |   |                                     |   |                        |                        |          |          |
|                                     | 11           | 10                                  | (1s) <sup>1</sup>                                     | <sup>2</sup> S <sub>1/2</sub>       | 16 ± 2  | 13 ± 3                 | 12 ± 3                 |          |          |
|                                     |              |                                     | (2s) <sup>1</sup>                                     | <sup>2</sup> S <sub>1/2</sub>       | 2   | 2                      | 2                      |          |          |
|                                     | 10           | 36                                  | zero-field configurations                             |                                     |   | } 33 ± 2 <sup>c)</sup> | } 17 ± 3 <sup>d)</sup> | } 21 ± 6 |          |
|                                     |              |                                     | (1s) <sup>1</sup> (2s) <sup>1</sup>                   | <sup>3</sup> S <sub>1</sub>         | } 19 ± 4  |                        |                        |          | } 9 ± 11 |
|                                     |              |                                     | (1s) <sup>1</sup> (2p) <sup>1</sup>                   | <sup>1</sup> P <sub>2</sub>         |   |                        |                        |          |          |
|                                     |              |                                     |   | <sup>3</sup> P <sub>1</sub>         | } 8 ± 8   |                        |                        |          |          |
|                                     |              | <sup>3</sup> P <sub>0</sub>         |   |                                     |   |                        |                        |          |          |
|                                     | 9            | 38                                  | (1s) <sup>2</sup> (2s) <sup>1</sup>                   | <sup>2</sup> S <sub>1/2</sub>       | } 10  | } 10                   | } 10                   |          |          |
|                                     |              |                                     | (1s) <sup>1</sup> (2s) <sup>1</sup> (2p) <sup>1</sup> | <sup>1</sup> P <sub>1,1,1</sub>     |   |                        |                        |          |          |
| (1s) <sup>1</sup> (2p) <sup>2</sup> |              |                                     | <sup>1</sup> P <sub>1,1,1</sub>                       |                                     |   |                        |                        |          |          |
| 8                                   | 12           | (1s) <sup>2</sup> (2s) <sup>2</sup> | <sup>1</sup> S <sub>0</sub>                           |                                     |   |                        |                        |          |          |
|                                     |              | <sup>e)</sup>                       |   | <sup>e)</sup>                       | Spectrograph <sup>b)</sup>  |                        |                        |          |          |
| <sup>20</sup> Ne                    | 10           | 4                                   | 6 ± 3   |                                     |   |                        |                        |          |          |
|                                     | 9            | 28                                  | 40 ± 5  | (1s) <sup>1</sup>                   | <sup>2</sup> S <sub>1/2</sub>   | 26 ± 8                 | 36 ± 5                 |          |          |
|                                     |              |                                     |   | (2s) <sup>1</sup>                   | <sup>2</sup> S <sub>1/2</sub>   | 4                      | 4 ± 1                  |          |          |
|                                     | 8            | 49                                  | 44 ± 4  | zero-field configurations           |   |                        | } 31 ± 8               | } 28 ± 3 |          |
|                                     |              |                                     |   | (1s) <sup>1</sup> (2s) <sup>1</sup> | <sup>3</sup> S <sub>1</sub>   | } 16 ± 2               |                        |          |          |
|                                     |              |                                     |   | (1s) <sup>1</sup> (2p) <sup>1</sup> | <sup>3</sup> P <sub>2,1</sub>   |                        |                        |          |          |
| 7                                   | 19           | 10 ± 3                              | (1s) <sup>2</sup> (2s) <sup>1</sup>                   | <sup>2</sup> S <sub>1/2</sub>       | } 8   | } 8 ± 3                |                        |          |          |
|                                     |              |                                     | (1s) <sup>1</sup> (2s) <sup>1</sup> (2p) <sup>1</sup> | <sup>1</sup> P <sub>1,1,1</sub>     |   |                        |                        |          |          |
|                                     |              |                                     | (1s) <sup>1</sup> (2p) <sup>2</sup>                   | <sup>1</sup> P <sub>1,1,1</sub>     |   | 2 ± 1                  |                        |          |          |

<sup>a)</sup> Simplified Marion and Young <sup>25)</sup> type calculation <sup>4,2)</sup>

<sup>b)</sup> Fits I to III are explained in subject. 3.4.1.

<sup>c)</sup> Statistically distributed: 9 %, 15 %, 9 %.

<sup>d)</sup> Statistically distributed: 11 %, 6 %.

<sup>e)</sup> Ref. <sup>25)</sup>.

<sup>f)</sup> Average of two integral spectrograph measurements. The errors were estimated from the spread in values obtained for two measurements.

<sup>g)</sup> Weighted mean of the results with the two targets.

<sup>h)</sup> Integral spectrograph measurement described in subject. 3.4.3.

$\gamma$ -ray angular correlations were measured for each charge state separately. The <sup>20</sup>Ne ions produced in the reaction <sup>12</sup>C(<sup>12</sup>C,  $\alpha$ )<sup>20</sup>Ne with charges from 7+ to 10+ were separated in an Enge-type split-pole spectrograph at an angle of 9° to the beam direction and were detected simultaneously in four position-sensitive detectors (one for each charge state) in coincidence with  $\alpha$ -particles detected at  $\phi_\alpha = 135^\circ$  to the beam direction. Gamma rays were detected in three 12.7 cm diam. by 12.7 cm long NaI(Tl) detectors in coincidence with  $\alpha$ -particles and <sup>20</sup>Ne ions. Two NaI(Tl) detectors were rotated in the (x, y) reaction plane between angles  $\phi = 55^\circ$  and  $120^\circ$  and  $\phi = 215^\circ$  and  $275^\circ$  to the beam direction (x-axis). The third detector was set in two positions out of the reaction plane at angles  $\theta = 0^\circ$  and  $\theta = 25^\circ$ ,  $\phi = 120^\circ$ .

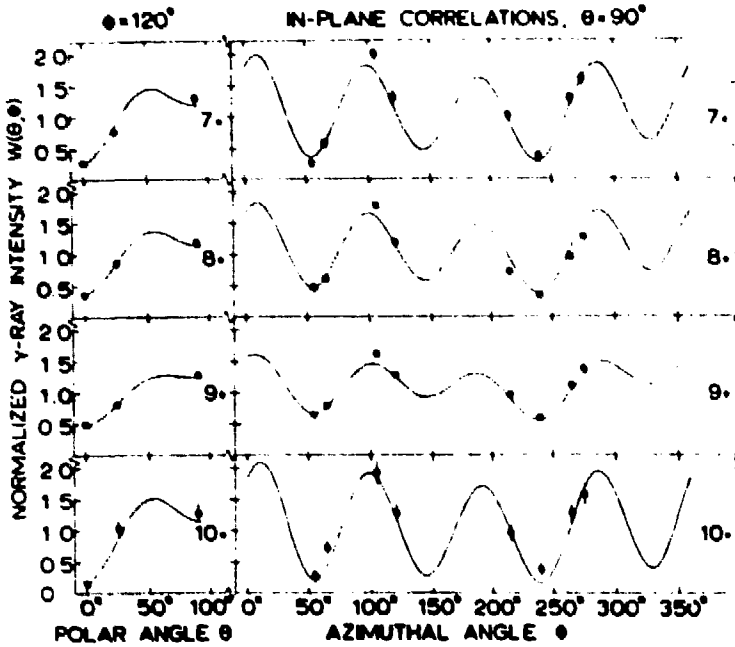


Fig. 13. Measured  $\gamma$ -ray angular correlations for the 7+ to 10+ ionic charge states of  $^{20}\text{Ne}$  separated with a magnetic spectrograph. The  $z$ -axis is perpendicular to the horizontal ( $x, y$ ) reaction plane defined by the beam direction and the  $^{20}\text{Ne}$  detection angle ( $9^\circ$  to the beam direction). The correlations were measured out of the reaction plane at an azimuthal angle of  $\phi = 120^\circ$  as well as in the reaction plane (polar angle  $\theta = 90^\circ$ ). The curves represent a simultaneous fit to the data as described in subject. 3.4.3.

The  $\gamma$ -ray angular correlations measured for the four charge states are displayed in fig. 13. The data were fitted with eq. (6) with the inclusion of corrections for the finite opening angle of both the  $\gamma$ -ray detectors ( $Q_k$  coefficients) and the spectrograph and for the relativistic velocity of the  $^{20}\text{Ne}$  nuclei. For each charge state only the population of the ground state and one excited state were taken into account. This is discussed below. The time-integral deorientation coefficients  $G_k(\infty)$  for each electronic state were taken from eq. (5) for infinite time and for the value of the  $g$ -factor given in table 3. The density matrix elements in eq. (7) [four free parameters, i.e. two relative substate populations and two phase factors  $^{10}$ ], the relative populations of each ground and excited state (three parameters) and the normalization factor were determined from a simultaneous fit to all the measured correlations (40 data points). For single-electron ions only  $1s$  and  $2s$  configurations were included and for two-electron ions the populations of the  $^3S_1$ ,  $^3P_2$  and  $^3P_1$  states were assumed to be statistical. For three-electron ions, in order to explain the rather large perturbation measured, it was found necessary to introduce an excited state with an unpaired  $1s$  electron, in addition to the  $(1s)^2(2s)^1$  ground state. Such a state might be given by the configurations  $(1s)^1(2s)^1(2p)^1$ ,  $(1s)^1(2p)^2$ ; ( $^4P$ ), see for examples refs. 23, 24).

The populations of the configurations obtained in this experiment and the charge state fractions extracted at the same time from the data are given in table 4. The agreement with the populations extracted from the time-differential data is excellent. The measured charge state fractions may also be compared with those calculated semi-empirically by Marion and Young<sup>25</sup>). There is a slight shift in the calculated charge distribution towards higher charge states. This could be due to the dependence of the charge distribution on the density and the atomic number of the target material<sup>26</sup>). For example, a plunger experiment carried out with  $^{24}\text{Mg}$  ions recoiling through a thin layer of Ag showed a much lower population of the  $(1s)^1$  state. Furthermore, a time-integral measurement in the slit geometry for  $^{24}\text{Mg}$  on recoil through thin layers of various metals showed a marked dependence on the atomic number of the layer. Hence the experimental values for the charge state fractions in table 4 are to be preferred.

The spectrograph experiment showed that  $(63 \pm 3)\%$  of two-electron Ne ions at  $v/c = 5.7\%$  are in an excited state with a strong hyperfine interaction;  $(90 \pm 3)\%$  of the one-electron ions and  $(80 \pm 6)\%$  of the three-electron ions, however, are in their ground states. This surprisingly high fraction of two-electron excited ions was deduced with the value of the  $g$ -factor taken from the plunger experiment; the population from the plunger experiment itself with the total fraction (table 4) yielded an excited fraction of  $(70 \pm 20)\%$ . Similar fractions may be deduced for Mg ions from the data in table 4, although a spectrograph experiment has not been carried out.

A similar spectrograph experiment was performed by Goldring *et al.*<sup>2)</sup> for  $^{18}\text{O}$  ions at about the same time as the  $^{20}\text{Ne}$  experiment. The rotation of the angular correlation due to non-axial detection of the reaction products was compensated by shifting the symmetry axis deduced from the angular correlation with respect to the beam direction. The data were interpreted under the assumption of axial symmetry. This approximation alone, however, is not sufficient to account for the fact that the value (14–37%) deduced for the population of excited two-electron states with a strong hyperfine interaction is appreciably lower than that deduced from the Ne experiment. The reason for this difference is not at present understood.

**3.4.4. The lifetime measurements.** The Ge(Li) detector at  $0^\circ$  to the beam direction served as a check on the lifetimes of the first-excited states. For  $^{24}\text{Mg}$  the data were sufficiently good for a precision measurement. For  $^{20}\text{Ne}$ , however, due to instability of the Ge(Li) detector caused by high counting rates and neutron damage, the data were not further analyzed. From the  $g$ -factor fits with the NaI(Tl) detectors values for the lifetimes were also extracted (see subsect. 3.4.2).

For  $^{24}\text{Mg}$  the stopped fractions, i.e. the fractions of  $\gamma$ -rays detected from nuclei decaying in the stopper, are displayed as a function of target-stopper distance in fig. 14. Analysis of these data leads to a mean life of  $\tau_m = 2.09 \pm 0.13$  ps. This value deviates from the compiled<sup>27)</sup> value ( $1.75 \pm 0.08$  ps), but agrees well with more recent measurements<sup>28)</sup>. The various corrections included in the analysis are discussed below.

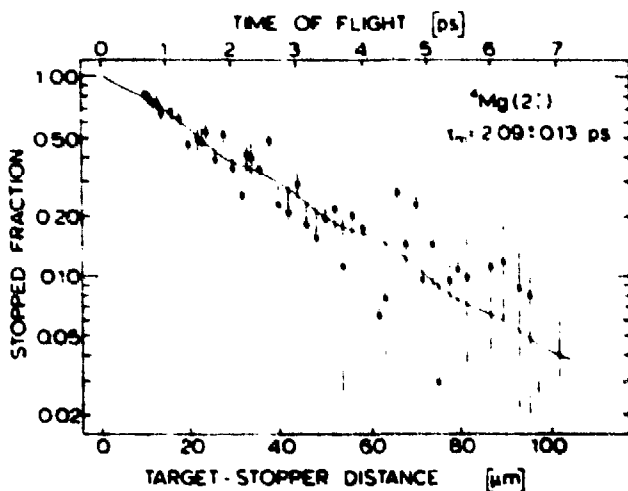


Fig. 14. Fractions of  $^{24}\text{Mg}^*$  nuclei decaying in the stopper as a function of perpendicular target-stopper distance measured with a Ge(Li) detector at  $0^\circ$  to the beam direction. The lifetime was determined by a least-squares fit to the data. The oscillation of the curve arises from the inclusion of deorientation effects calculated from the values of the  $g$ -factor and the populations of electronic states from the present work. The increasing errors towards larger target-stopper distances reflect the equal measuring time for each point necessary for an optimum determination of the  $g$ -factor.

Since the nuclear lifetime is comparable to the slowing-down time of the nuclei in the stopper, the tail of the stopped peak line-shape contributes to the intensity at the flight peak position. The correction on the intensity of the flight peak was estimated as follows. First the spectra were corrected for multiple Compton scattering of  $\gamma$ -rays emitted in flight. The line-shape of the stopped fraction was then extrapolated with a standard line-shape program<sup>29)</sup> to determine the contribution under the flight peak. This correction was always less than 6%. The contents of the flight peak were further corrected for relativistic effects on both the opening angle and the efficiency of the Ge(Li) detector. Deorientation effects were also taken into account in the least-squares fit to the data, although these effects are small at  $0^\circ$  (less than 10%) in the present case. The values of the  $g$ -factor and of the populations of the electronic states were taken from the present work. The best  $\chi^2$  value for the fit was obtained for the same zero distance (with an error of  $1.3 \mu\text{m}$ ) as measured by eye. The weighted mean from four independent zero-distance measurements (see subsect. 3.4.2) was taken in the lifetime fit.

## 4. Theoretical discussion and conclusions

### 4.1. THEORETICAL DISCUSSION

Theoretical calculations of  $g$ -factors for the first-excited states of  $^{24}\text{Mg}$  and  $^{20}\text{Ne}$  are compared with the present experimental results in table 5.

For  $^{24}\text{Mg}$  the single-shell ( $1d_{3/2}$ ) and the modified surface delta interaction (MSDI) two-shell ( $1d_{3/2}2s_{1/2}$ ) calculations<sup>30)</sup> differ by more than three standard deviations from



TABLE 5  
Comparison of theoretical  $g$ -factors with experiment

|                                       | $g$ -factor             |                         |
|---------------------------------------|-------------------------|-------------------------|
|                                       | $^{20}\text{Ne}(2_1^+)$ | $^{24}\text{Mg}(2_1^+)$ |
| Experiment                            | $\pm 0.54 \pm 0.04$     | $-0.51 \pm 0.02$        |
| PHF <sup>a)</sup>                     | $-0.54$                 | $-0.55$                 |
| PHF <sup>b)</sup>                     |                         | $-0.57$                 |
| SU(3) <sup>c)</sup>                   |                         | $-0.50$                 |
| Shell model calculations:             |                         |                         |
| Single shell ( $1d_3$ ) <sup>d)</sup> |                         | $-0.58$                 |
| MSDI ( $1d_3 2s_4$ ) <sup>e)</sup>    |                         | $-0.57$                 |
| Truncated: KLS <sup>f)</sup> ,        |                         | $-0.52$                 |
| MSDI/PW/Kuo/ASDI <sup>g)</sup>        |                         | $-0.52$ to $-0.54$      |
| Full space: MSDI <sup>h)</sup> ,      | $-0.51$                 |                         |
| MSDI/PW/Kuo <sup>i)</sup>             | $-0.51$                 | $-0.51$ to $-0.53$      |

<sup>a)</sup> Ref. <sup>31)</sup>,   <sup>b)</sup> Ref. <sup>32)</sup>,   <sup>c)</sup> Ref. <sup>33)</sup>,   <sup>d)</sup> Ref. <sup>30)</sup>,   <sup>e)</sup> Ref. <sup>34)</sup>,   <sup>f)</sup> Ref. <sup>33)</sup>,  
<sup>g)</sup> Ref. <sup>36)</sup>.

the experimental value. Projected Hartree-Fock (PHF) calculations <sup>31,32)</sup> also deviate significantly. The earlier experimental values for the  $g$ -factor <sup>10,12)</sup> ( $g = +0.44 \pm 0.04$ ) led to the inclusion of the  $1d_3$  configuration in the Utrecht calculations <sup>33)</sup>. These calculations in a truncated space with MSDI, Preedom-Wildenthal (PW), Kuo and adjusted surface delta interaction (ASDI) matrix elements lead to values in good agreement with the present experiment. Another calculation in a truncated space with renormalized Kahana-Lee-Scott (KLS) matrix elements <sup>34)</sup> and an SU(3) calculation <sup>35)</sup> also agree with the present data.

Calculations in the full ( $1d_3 2s_4 1d_3$ ) space all yield slightly lower values than the truncated calculations, in better agreement with the experimental value.

For  $^{24}\text{Mg}$  it may thus be concluded that the  $1d_3$  configuration contributes significantly to the  $g$ -factor of the first  $2^+$  state and that, as expected, calculations in the full  $sd$  space give somewhat better results. It is not yet possible to distinguish between various interactions for doubly even  $T = 0$  nuclei because neither the theoretical nor the experimental values are precise enough.

For  $^{20}\text{Ne}$  fewer calculations have been performed <sup>33,36)</sup> and the agreement with the experimental value is well within the experimental error.

## 4.2. CONCLUSIONS

The present paper shows that the time-differential recoil-into-vacuum technique can be used to measure  $g$ -factors of nuclei in excited states even for velocities at which only a 10–20% fraction of single-electron ions is present. The data also show that about 60% of the two-electron ions may be in an excited electronic state with a strong hyperfine interaction. This may enable the measurement of  $g$ -factors of higher- $Z$  nuclei at velocities at which only low fractions of two-electron ions are present.

The  $g$ -factor would then be determined mainly from the high-frequency component arising from the two-electron excited states. It has further been demonstrated that integral measurements with charge-state separation yield useful information on charge-state distributions and excitation probabilities. This information can be used to facilitate and improve the interpretation of time-differential experiments. It should be noted that the assumption of a statistical distribution for the population of electronic states with about the same excitation energy may not necessarily be valid (see subject 3.4.3).

It has been shown that the detection of particles in a slit-detector considerably improves the anisotropy of the  $\gamma$ -ray angular correlation for reactions with spinless particles for those cases in which the anisotropy for particle detection in an annular detector is spoiled by high angular momentum transfer from the incoming to the outgoing particle. In this geometry  $g$ -factors and also lifetimes of the order of 1 ps were determined, without separation of flight and stopped fractions, with high efficiency NaI(Tl) detectors at  $90^\circ$  to the beam.

The experimental value obtained for the  $g$ -factor of  $^{20}\text{Ne}$  may also be used to calibrate the transient field in the high-recoil-velocity region where large deviations from the empirically adjusted Lindhard and Winter theory<sup>9,37,38</sup>) have been observed.

### References

- 1) M. A. Faessler, B. Povh and D. Schwalm, *Ann. of Phys.* **63** (1971) 577
- 2) G. Goldring *et al.*, *Phys. Rev. Lett.* **28** (1972) 763
- 3) W. L. Randolph *et al.*, *Phys. Lett.* **44B** (1973) 36
- 4) T. K. Alexander *et al.*, *Phys. Rev.* **C9** (1974) 1748
- 5) J. R. Beene *et al.*, *Nucl. Phys.* **A230** (1974) 141
- 6) J. Asher *et al.*, *J. of Phys. G1* (1975) 415
- 7) H. A. Doubt *et al.*, *Proc. Int. Conf. on hyperfine interactions* (Upplands Graviska, Uppsala, 1974) p. 93
- 8) Z. Berant *et al.*, *Nucl. Phys.*, **A243** (1975) 519
- 9) J. L. Eberhardt, R. E. Horstman, H. A. Doubt and G. van Middelkoop, *Nucl. Phys.* **A244** (1975) 1;  
J. L. Eberhardt, G. van Middelkoop, R. E. Horstman and H. A. Doubt, *Phys. Lett.*; **56B** (1975) 329
- 10) R. E. Horstman, J. L. Eberhardt, H. A. Doubt and G. van Middelkoop, *Phys. Lett.* **48B** (1974) 31
- 11) H. J. Andr , *Physica Scripta* **9** (1974) 257
- 12) J. L. Eberhardt, R. E. Horstman, H. W. Heeman and G. van Middelkoop, *Nucl. Phys.* **A229** (1974) 162
- 13) N. Bohr, *Phys. Rev.* **58** (1940) 654; **59** (1941) 270
- 14) H. Frauenfelder and R. M. Steffen, in *Alpha-, beta-, and gamma-ray spectroscopy*, ed. K. Siegbahn, vol. 2 (North-Holland, Amsterdam, 1965)
- 15) H. Kopfermann, *Kernmomente* (Akademische Verlag, Frankfurt, 1956)
- 16) Z. Berant *et al.*, *Nucl. Phys.* **A178** (1971) 155
- 17) A. Bohr, *Nucl. Phys.* **10** (1959) 486

- 18) J. G. Cramer and W. W. Eidson, *Nucl. Phys.* **55** (1964) 591
- 19) F. Bosch and H. Spehl (Universität Freiburg), to be published
- 20) D. K. Olsen *et al.*, *Nucl. Phys.* **A220** (1974) 541
- 21) M. B. Goldberg, *Physica Scripta* **11** (1975) 184
- 22) C. P. Bhalla, D. L. Matthews and C. F. Moore, *Phys. Lett.* **46A** (1973) 336
- 23) D. J. Pegg *et al.*, *Phys. Rev.* **A9** (1974) 1112
- 24) C. F. Moore, W. J. Braithwaite and D. L. Matthews, *Phys. Lett.* **44A** (1973) 199
- 25) J. B. Marion and F. C. Young, *Nuclear reaction analysis* (North-Holland, Amsterdam, 1968)
- 26) H. H. Heckman, E. L. Hubbard and W. G. Simon, *Phys. Rev.* **129** (1963) 1240
- 27) P. M. Endt and C. van der Leun, *Nucl. Phys.* **A214** (1973) 1
- 28) C. Broude, F. A. Beck and P. Engelstein, *Nucl. Phys.* (1971) 603;  
 A. Johnston and T. E. Drake, *J. of Phys.* **A7** (1974) 898;  
 J. S. Forster *et al.*, *Phys. Lett.* **51B** (1974) 133;  
 D. Schwalm *et al.*, see E. K. Warburton, *Proc. Int. Conf. on nuclear structure and spectroscopy*,  
 vol. 2 (Scholar's Press, Amsterdam, 1974) p. 506;  
 S. F. Biagi, W. R. Phillips and A. R. Barnett, *Nucl. Phys.* **A242** (1975) 160
- 29) J. A. J. Hermans *et al.*, *Nucl. Phys.*, to be published
- 30) J. F. A. van Hienen and P. W. M. Glaudemans, *Phys. Lett.* **42B** (1972) 301
- 31) M. R. Gunye and C. S. Warke, *Phys. Rev.* **159** (1967) 885
- 32) M. R. Gunye, *Phys. Lett.* **37B** (1971) 125
- 33) G. A. Timmer, F. Meurders and J. F. Koops (Utrecht University), private communications
- 34) S. K. M. Wong, J. M. G. Gomez and A. P. Zuker, *Phys. Lett.* **42B** (1972) 157
- 35) D. Strottman, *Phys. Lett.* **39B** (1972) 457
- 36) E. C. Halbert, J. B. McGrory, B. H. Wildenthal and S. P. Pandya, *Advances in nuclear physics*,  
 vol. 4, ed. M. Baranger and E. Vogt (Plenum Press, New York, 1971) p. 316
- 37) M. Forterre *et al.*, *Phys. Lett.* **55B** (1975) 59
- 38) M. Forterre *et al.*, *Phys. Rev.* **C11** (1975) 1976
- 39) R. Marrus, *Nucl. Instr.* **110** (1973) 333
- 40) W. L. Wiese, M. W. Smith and B. M. Glennon, Report NSRDS-NBS 4 (1966) vol. 1;  
 W. L. Wiese, M. W. Smith and B. M. Miles, Report NSRDS-NBS 22 (1969) vol. 2
- 41) I. A. Sellin, M. Brown, W. W. Smith and B. Donnally, *Phys. Rev.* **A2** (1970) 1184
- 42) H. D. Betz, *Rev. Mod. Phys.* **44** (1972) 465;  
 A. B. Wittkower and H. D. Betz, *Atomic Data* **5** (1973) 113,  
 I. S. Dmitriev and V. S. Nikolaev, *JETP (Sov. Phys.)* **20** (1965) 409
- 43) Landolt-Börnstein, *Zahlenwerte und Funktionen*, Band I, Teil 1 (Springer, Berlin, 1950) p. 48

## CHAPTER II

# RECOIL-DISTANCE MEASUREMENT OF THE g-FACTOR OF $^{22}\text{Ne}(2_1^+)$ AND A TRANSIENT MAGNETIC FIELD CALIBRATION

**Abstract:** A time-differential recoil-into-vacuum measurement with a plunger has been performed on the first-excited  $2_1^+$  state of  $^{22}\text{Ne}$ . The state was populated with the  $^4\text{He}(^{19}\text{F}, p)^{22}\text{Ne}$  reaction on  $^4\text{He}$ -implanted foils. This experiment together with a transient field precession measurement to determine the sign of the g-factor leads to a value for the g-factor of  $g = +0.325 \pm 0.017$ . The mean life of the state has been determined as  $\tau = 5.2 \pm 0.3$  ps.

The analysis of the plunger data also yields the population of excited two-electron ions and there are indications that the population depends on the material through which the ions recoil into vacuum. Transient field precessions were measured at low and high recoil velocities. At high recoil velocity a large deviation from the Lindhard-Winther prediction has been found.

### 1. Introduction

It has been shown <sup>1)</sup> for the doubly even  $T=0$  nuclei  $^{20}\text{Ne}$  and  $^{24}\text{Mg}$  that shell-model calculations generally reproduce quite precisely the value of the g-factor of the first-excited state. For doubly even  $T=1$  nuclei, however, the calculated value for the g-factor is more sensitive on the effective two-body interaction and the configuration space <sup>2)</sup>. Recent measurements on the short-lived ( $\tau < 1$  ps) first-excited states of  $^{26}\text{Mg}$  and  $^{30}\text{Si}$  in this laboratory <sup>3,4)</sup> with the transient field method have shown to be very useful in this

respect. It was therefore thought worthwhile to investigate also the relatively long-lived first-excited state of  $^{22}\text{Ne}$  ( $\tau = 4.9$  ps) at  $E_x = 1.27$  MeV with the accurate time-differential deorientation method <sup>1,5)</sup>.

The sign of the g-factor was determined from a spin precession measurement on recoil into magnetized iron. This method employs the transient magnetic field <sup>3,6)</sup>.

The recently found anomalously high transient fields for light nuclei <sup>7-9)</sup> and the increase of these fields with recoil velocity <sup>10)</sup>, which deviates largely from the velocity dependence calculated by Lindhard and Winther <sup>11)</sup>, was also investigated in the present paper by measuring time-integral precessions at velocities of  $v/c = 0.015$  and  $0.049$ . The absolute value of the g-factor from the time-differential measurement also gave an absolute calibration of the transient magnetic field at the two velocities.

## 2. Description of the experiments

### 2.1. THE RECOIL-DISTANCE MEASUREMENTS

Time-differential deorientation measurements make use of the static hyperfine interaction in free highly-ionized atoms recoiling out of a target foil into vacuum. The resulting periodic dealignment and alignment of the initially aligned spins of a nuclear excited state, reflected in periodic changes of the angular distribution of  $\gamma$ -rays emitted by the excited nuclei, is detected time-differentially by means of a plunger, see e.g. ref. <sup>1)</sup>. As the hyperfine interaction has no preferential direction it is not possible to determine the sign of the g-factor.

The first-excited state of  $^{22}\text{Ne}$  was populated by the

heavy-ion reaction  ${}^4\text{He}({}^{19}\text{F},\text{p})$  to obtain the necessary high ionization of the  ${}^{22}\text{Ne}$  ions. The plunger target foils (see also subsect. 2.3), which consist of  ${}^4\text{He}$ -implanted  $500\ \mu\text{g}/\text{cm}^2$  Ni onto  $300\ \mu\text{g}/\text{cm}^2$  Ag, the latter added for good heat conduction, were mounted with the Ni facing the stopper and were bombarded with  $40.6\ \text{MeV}\ {}^{19}\text{F}^{+6}$  ions from the Utrecht 7 MV EN tandem Van de Graaff accelerator. This energy was chosen for an optimum in yield and experimental anisotropy in the  $2_1^+ \rightarrow 0_1^+$   $\gamma$ -ray angular distribution.

Gamma-rays were detected in coincidence with protons in four  $12.7\ \text{cm}$  diam. by  $12.7\ \text{cm}$  long NaI(Tl) scintillation crystals at angles of  $45^\circ$ ,  $90^\circ$ ,  $-90^\circ$  and  $-135^\circ$  with respect to the beam direction and at distances of  $16\ \text{cm}$  from the target. A  $125\ \text{cm}^3$  Ge(Li) detector was placed at  $0^\circ$  and at a distance of  $11.5\ \text{cm}$  to measure the lifetime of the state and the recoil velocity of the  ${}^{22}\text{Ne}$  nuclei. Protons were detected at  $0^\circ$  in a  $2\ \text{mm}$  thick Si surface-barrier detector with an opening angle of  $17^\circ$ , shielded with a  $120\ \mu\text{m}$  thick Au foil. The experimental set-up of the detectors and the plunger assembly is described in detail in ref.<sup>1)</sup>. Some details relevant to the present experiment are given here.

For proton detection at  $0^\circ$  the massive stopper [see ref.<sup>1)</sup>] was replaced by a  $30\ \mu\text{m}$  thick Au stopper foil stretched over a  $2.7\ \text{mm}$  diam. stainless steel cylinder precisely fitting in the cylinder over which the target foil was stretched. The plunger assembly was mounted at  $30^\circ$  to the beam direction such that protons could be detected at  $0^\circ$  through a slit in both cylinders. This is schematically shown in fig. 1. The stability and flatness of the target foil were continuously monitored during the experiment by means of a laser interfer-

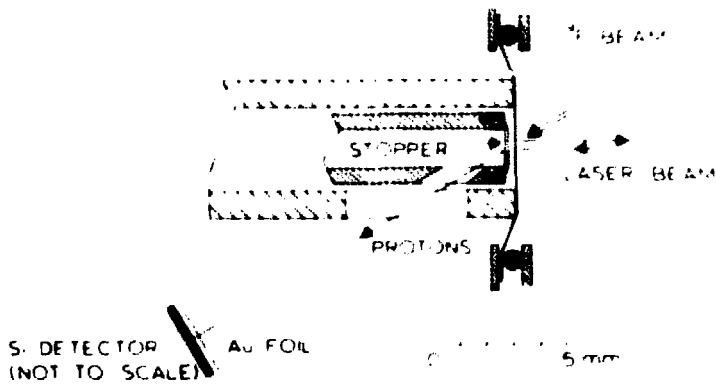


Fig. 1. Schematic cross section of the plunger assembly showing the He-implanted target foil, the 30  $\mu\text{m}$  thick stopper foil and the proton detector at  $0^\circ$  to the beam direction. The laser beam reflecting on the target foil, which is part of an interferometer, is also shown.

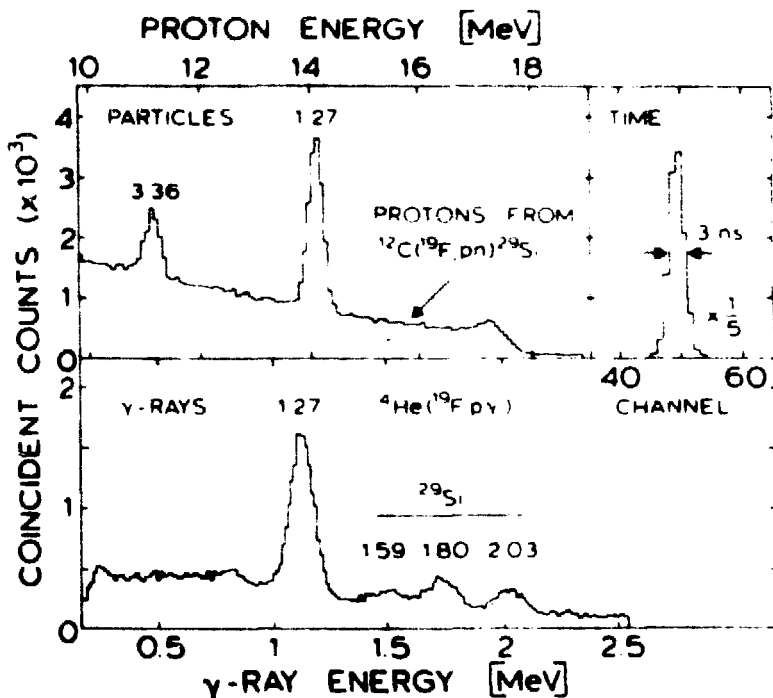


Fig. 2. Coincident particle,  $\gamma$ -ray and time spectra for the  $^4\text{He}(^{19}\text{F}, \text{py})^{22}\text{Ne}$  reaction summed over several runs. The backgrounds in the proton and  $\gamma$ -ray spectrum are mainly due to the contaminant  $^{12}\text{C}(^{19}\text{F}, \text{pn})^{29}\text{Si}$  reaction.

rometer. It was not possible, however, to monitor the position and the stability of the stopper foil. The flatness of this foil was checked several times in the experiments by opening the plunger assembly. The maximum allowable beam current varied depending on target conditions between 25 and 50 nA.

Carbon deposited on the target foil during the implantation and during the experiment caused a linear background in the particle spectra due to protons from the  $^{12}\text{C}(^{19}\text{F},\text{pn})^{29}\text{Si}$  and  $^{12}\text{C}(^{19}\text{F},\text{ap})^{26}\text{Mg}$  reactions. This is indicated in fig. 2, in which typical coincident particle,  $\gamma$ -ray and time spectra are shown.

Three independent measurements were performed. In the first and the second measurement one target foil was used each time. In the third experiment five foils were used in an attempt to keep the carbon contamination as low as possible. Each experiment required 5 d of beam time. The plunger distance was changed approximately every 1.5 h.

The data were collected by means of an on-line computer system with associated electronics as described in detail in ref. 1).

## 2.2. THE TRANSIENT FIELD SPIN-PRECESSION MEASUREMENTS

When ions of (excited) nuclei recoil into a magnetized ferromagnetic material (e.g. Fe) these nuclei experience during slowing down strong magnetic fields, so-called transient fields <sup>11)</sup>, which are thought to be caused by the scattering of polarized electrons of the ferromagnet in the Coulomb potential of the moving ion. The increased density of polarized electrons near the nucleus causes an enhanced magnetic field. In this model, developed by Lindhard and



Winther <sup>11)</sup> (LW), this enhancement was shown to be proportional to the average of the inverse of the orbital velocity  $v_p$  of 3d electrons in Fe for recoil velocities  $v < v_p$  and proportional to  $1/v$  for  $v > v_p$ . By adjusting  $v_p$  as a parameter good agreement was obtained with the experimentally determined transient fields for  $Z \geq 26$  nuclei in Fe at recoil velocities of  $v/c \approx 0.015$ . Transient fields in Fe for  $Z \geq 26$  nuclei were calculated with this empirically adjusted theory (ALW) and used in several experiments to determine g-factors, see refs. <sup>3,4,6)</sup>.

It was recently observed <sup>9,10)</sup> that at higher recoil velocities the transient fields are much larger than the LW theory predicts. Since the absolute value of the g-factor of the first-excited  $2^+$  state of  $^{22}\text{Ne}$  was determined precisely and independently by a deorientation measurement (see sect. 3) the transient field measurements served a dual purpose, i.e. to determine the sign of the g-factor and to calibrate the transient field of  $^{22}\text{Ne}$  in Fe at two velocities. The latter information is of importance for tracing the origin of the anomalously strong fields and for future experiments with these fields on extremely short-lived nuclear states (i.e.  $\tau \approx 100$  fs).

Since the transient field is aligned with the external magnetic field, which polarizes the Fe foil, the nuclear spins will precess about the field axis which precession is measured time-integrally as a small rotation of the angular distribution of  $\gamma$ -rays emitted by the nuclei in an excited state.

Low-recoil velocity ( $v/c = 0.015$ )  $^{22}\text{Ne}$  nuclei in the first-excited state were produced with the  $^{19}\text{F}(\alpha, p)$  reaction by

bombarding a  $200 \mu\text{g}/\text{cm}^2$  LiF layer evaporated onto a Fe backing of  $10 \mu\text{m}$  with  $8.06 \text{ MeV } ^4\text{He}^+$ -particles from the Utrecht tandem accelerator. Outgoing protons were detected with an annular Si-surface barrier detector, which subtended angles between  $168^\circ$  and  $175^\circ$  to the beam direction, shielded with a  $50 \mu\text{m}$  thick mylar foil to stop backscattered  $\alpha$ -particles. Typical particle,  $\gamma$ -ray and time spectra are shown in fig. 3. The beam current was kept below  $100 \text{ nA}$  to prevent an appreciable decrease of reaction yield due to evaporation of the LiF target.

A target consisting of  $300 \mu\text{g}/\text{cm}^2$  LiF evaporated onto  $0.5 \text{ mm}$  Cu was used to measure the rotation of the  $\gamma$ -ray angular distribution due to the bending of the in- and outgoing  $\alpha$ -particle trajectories by the fringing field of the magnet used to polarize the Fe targets. This so-called "beam-bending

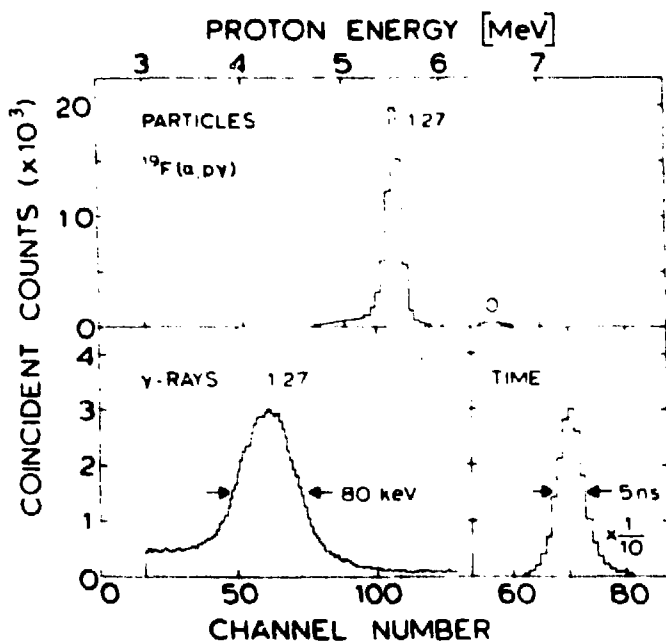


Fig. 3. Coincident particle,  $\gamma$ -ray and time spectra for the  $^{19}\text{F}(\alpha, p)^{22}\text{Ne}$  reaction used in the low-velocity transient field experiment.

effect" was subtracted from the effect observed with the Fe-backed targets.

The inverse reaction  ${}^4\text{He}({}^{19}\text{F},\text{p})$  at  $E({}^{19}\text{F}) = 38.5$  MeV was used to obtain  ${}^{22}\text{Ne}(2_1^+)$  nuclei at high recoil velocity ( $v/c = 0.049$ ). The protons were detected at  $0^\circ$  in a 2 mm thick Si surface-barrier detector with an opening angle of  $13^\circ$  shielded with a 120  $\mu\text{m}$  Au foil. This detector was mounted at the position of the cup shown in fig. 2 of ref. <sup>3)</sup>. The targets consisted of either a He-implanted 150  $\mu\text{g}/\text{cm}^2$  Ti layer or a He-implanted 40  $\mu\text{g}/\text{cm}^2$  Ta layer on 5  $\mu\text{m}$  Fe foils, onto which 6  $\text{mg}/\text{cm}^2$  Ag was evaporated for heat conduction. A target of He implanted 25  $\mu\text{m}$  thick Ta with a 6  $\text{mg}/\text{cm}^2$  Ag backing was used to measure the beam bending.

The beam current was kept below 250 nA to prevent escape of the He from the target.

In both experiments  $\gamma$ -rays were detected in coincidence with protons in four 12.7 cm diam. by 12.7 cm long NaI(Tl) crystals at the rotation sensitive angles  $+72^\circ$  and  $+108^\circ$  to the beam direction and at 20 cm distance from the target. The experimental set-up is described in detail in ref. <sup>3)</sup>. The Fe-backed targets were shifted in position every 6 h, to prevent radiation damage of the Fe. The polarizing external magnetic field  $B = 0.15$  T was reversed every 2 min, to prevent possible systematic effects. The on-line computer-controlled data collection system and the electronics are described in refs. <sup>1,3)</sup>.

### 2.3. TARGET PREPARATION

The He targets were prepared through implantation by means of an ion source with 30 kV extraction. The target foils were bombarded with  ${}^4\text{He}^+$  particles during 4 h at a beam current

of  $10 \mu\text{A}/\text{cm}^2$ . Helium was implanted in the Ni layers of the plunger foils or in Ti and Ta layers for the transient field measurements.

After the implantation the irradiated area of the Ni-Ag plunger foils appeared to have expanded. To be able to stretch this area on mounting such a foil in the plunger it was found necessary to collimate the He beam to 5 mm diam.

The iron foils\* for the transient field experiments were annealed for half an hour in a 200 Torr  $\text{H}_2$  atmosphere at about  $700^\circ\text{C}$ . This process also reduces the oxide layer on the foils. Without exposing the foils to air again this process was immediately followed by vacuum evaporation of Ti, Ta or LiF.

### 3. Results and interpretation

#### 3.1. THE RECOIL-DISTANCE MEASUREMENTS

The ratio  $R(t)$  of coincident  $\gamma$ -ray counts (the  $\gamma$ -ray anisotropy) measured at  $\pm 90^\circ$  to those at  $45^\circ$  and  $-135^\circ$  corrected for absorption in the target chamber, for detector efficiencies and for coincident background is shown as a function of time, i.e. target-stopper distance, in fig. 4 for the three experiments. The uncertainties in the target-stopper distance and the "zero distance" were estimated to be  $2 \mu\text{m}$ . The zero distance  $d_0$  was measured by eye as described in ref.<sup>1)</sup> and consistent values were found from fits to  $R(t)$  with  $d_0$  as a free parameter. Although the laser interferometer monitor showed no variations in target foil position during the expe-

\* Manufactured by Ventron Corp., Massachusetts, U.S.A. and by Goodfellow Metals Ltd., Esher, Surrey, England.

riments of more than 0.5  $\mu\text{m}$ , the target-stopper distance might have varied by larger non-observed stopper displacements due to heating by the beam. An estimate of these displacements was obtained in the following way.

Regularly the stopper was set to within 1  $\mu\text{m}$  from touching the target and no change in target foil position between beam off and on could be detected. This indicated a good stability of the stopper foil, since thermal expansion of this foil would most probably decrease the target-stopper distance because the stopper is somewhat convex as it is a thick foil stretched over a small diameter.

The flight time was calculated from the target-stopper distance with the ion velocity determined from the Doppler shift observed with the Ge(Li) detector. This velocity found to be  $v/c = 0.0484 \pm 0.0002$  is in good agreement with the calculated value from kinematics and stopping powers<sup>12)</sup>.

The experimental ratios  $R(t)$  were first fitted with the calculated (oscillatory) function for the time-dependent de-orientation from hydrogen-like ions together with a fixed fraction<sup>13)</sup> of 30 % Li-like ions in their ground states, see ref.<sup>1)</sup>. This resulted in poor fits with  $\chi^2$  exceeding 2. Inclusion of contributions from isomeric (i.e. with lifetime longer than the nuclear lifetime) excited helium-like ions improved the fits appreciably with  $\chi^2$  values between 1 and 1.2, without changing the values for the g-factor. The data were not sufficiently good to determine the individual contributions of the  $1s2s$  configuration coupled to  $^3S_1$  and the  $1s2p$  configurations coupled to  $^3P_1$  or  $^3P_2$ . Therefore the contributions were assumed statistically distributed proportional to  $2J+1$ , where  $J$  is the total angular momentum of the two electrons.

In the final fits a fixed fraction of lithium-like ions in the ground state of 20 - 30 % was included. This did not change the value of the g-factor by more than a fifth of the standard deviation.

The analyses led to three mutually consistent values of the g-factor for  $^{22}\text{Ne}(2_1^+)$ . In the final errors the uncertainties in the zero distance, the ion velocity, the nuclear lifetime and the hyperfine-coupling constants were included. The nuclear lifetime was taken as  $\tau = 5.0 \pm 0.2$  ps, which is the average of the present (see below) and a compiled value [ref. <sup>14</sup>)], and the hyperfine-coupling constants for  $^{20}\text{Ne}$  were used <sup>1)</sup>. This resulted in a value of the g-factor of  $|g| = 0.325 \pm 0.017$ .

TABLE I

Results from the fits to the R(t)-values

| Target           | Populations of electronic states (%) |            |    | $\chi^2$ | $ g $                   |
|------------------|--------------------------------------|------------|----|----------|-------------------------|
|                  | 9+                                   | excited 8+ | 7+ |          |                         |
| 1                | $31 \pm 6$                           | $8 \pm 9$  | 20 | 1.15     | $0.303 \pm 0.020$       |
| 2                | $7 \pm 5$                            | $25 \pm 5$ | 30 | 1.07     | $0.351 \pm 0.032$       |
| 3                | $7 \pm 5$                            | $28 \pm 8$ | 30 | 1.00     | $0.352 \pm 0.030$       |
| average g-factor |                                      |            |    |          | $ g  = 0.325 \pm 0.017$ |

Table I lists the populations found for the different electronic configurations. For targets 2 and 3 this shows again the

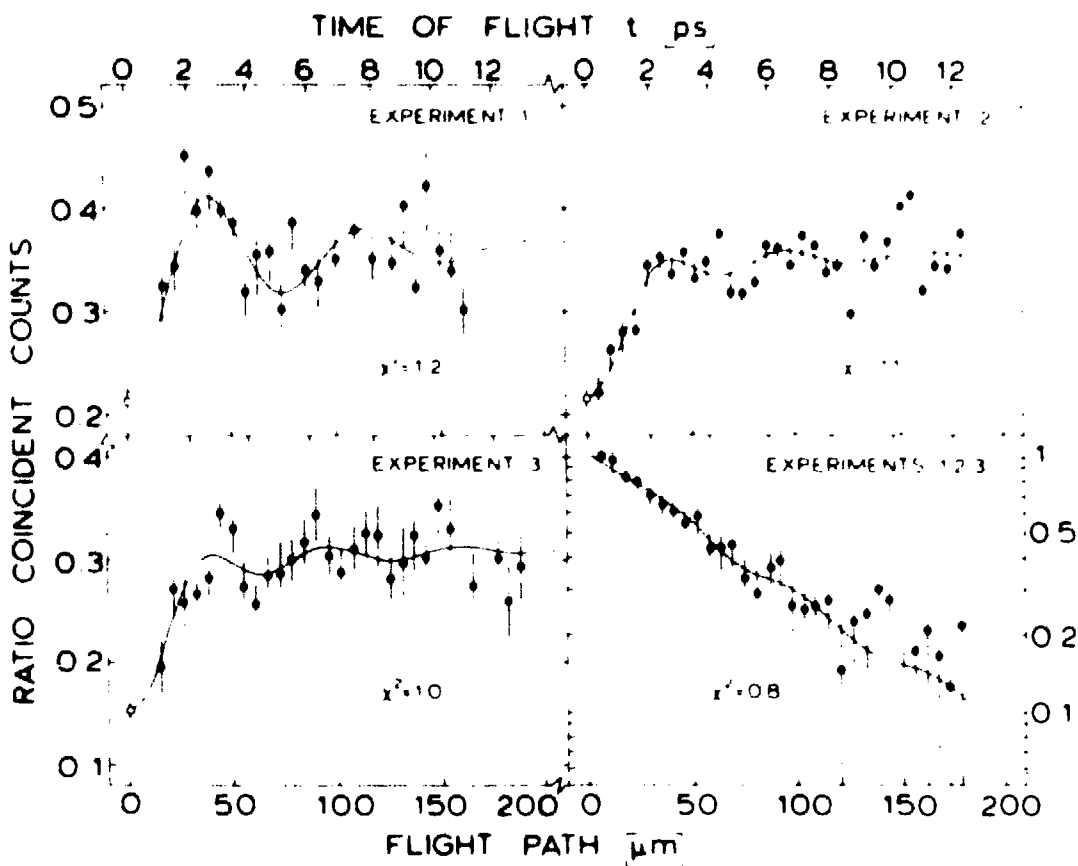


Fig. 4. Ratio of coincident counts  $R(t)$  as a function of target-stopper flight path for the three  $g$ -factor experiments separately. The oscillatory curves are least-squares fits to these ratios. The fraction of  $^{22}\text{Ne}(2_1^+)$  nuclei decaying in the stopper measured with a Ge(Li) detector at  $0^\circ$  to the beam direction is also shown. The data from the three experiments are summed and the curve shown is for a mean life of  $\tau = 5.2$  ps, which is the weighted average of the lifetimes from the three experiments separately.

high fraction of excited states of the helium-like ions, which was also observed for  $^{20}\text{Ne}$  and  $^{24}\text{Mg}$ , see ref. 1). The results of target 1 show an entirely different behaviour. The fraction of ground state H-like ions is four times as large as for the other two targets, whereas the fraction of excited He-like ions is not significant. The differences are very likely due to the relatively large carbon deposit on target 1, whereas targets 2 and 3 had relatively clean Ni surfaces. It was observed earlier that the charge-state distribution shifts towards higher charge for decreasing atomic number of the target foil <sup>1,15)</sup>, which could account for the large fraction of H-like ions observed for target 1 where the ions recoil through carbon. The much lower fraction of excited He-like ions for target 1 might also be due to the carbon, although the process is not at present understood.

The fraction of ground-state Li-like ions was taken as 20 % for target 1 and as 30 % for targets 2 and 3. The value of the g-factor is insensitive to these fractions.

The coincident  $\gamma$ -ray spectra measured with the Ge(Li) detector at  $0^\circ$  to the beam direction as a function of target-stopper distance were also used for a determination of the mean life of the first-excited state in  $^{22}\text{Ne}$  at 1.27 MeV. The data, however, are rather poor since (i) the large  $\gamma$ -ray anisotropy (the population of the  $m=0$  magnetic substate was larger than 85 %) in this case leads to a minimum  $\gamma$ -ray yield at  $0^\circ$  and (ii) the measuring times for all distances were about equal, which is optimal for a g-factor measurement but not for a lifetime determination.

In fig. 4 also the fraction of nuclei decaying in the stopper is shown as a function of plunger distance for the three



measurements together. In the analysis the three measurements were treated independently and their results were averaged. The data analysis included corrections for opening angle and efficiency of the Ge(Li) detector and for deorientation. The latter is known from the g-factor analysis. The lineshape of the stopped fraction was also accounted for.

The analysis leads to three mutually consistent values with a weighted mean of  $\tau = 5.2 \pm 0.3$  ps in agreement with the compiled <sup>14)</sup> value of  $\tau = 4.9 \pm 0.3$  ps.

### 3.2. THE TRANSIENT FIELD MEASUREMENTS

The time-integral rotation of the  $\gamma$ -ray angular correlation, due to the precession of the nuclear spin in the transient field, was determined from the numbers of coincident counts  $N$  accumulated in the four  $\gamma$ -ray detectors at angles  $\pm(\frac{1}{2}\pi \pm \theta_1)$  for the polarizing external magnetic field up and down. The optimum detection angle, for full alignment of the  $2_1^+$  state, is  $\theta_1 = 18^\circ$  [see ref. <sup>3)</sup>]. To first order in the angle  $\theta$  and to second order in the effect  $\epsilon$  the rotation angle  $\Delta\theta$  can be expressed by

$$\Delta\theta = \frac{-1 + \sqrt{2\epsilon + 1}}{4} W(\theta) / \frac{dW(\theta)}{d\theta}, \quad (1)$$

where  $W(\theta)$  is the angular correlation function and the measured effect  $\epsilon$  for e.g. the detector pair at  $\frac{1}{2}\pi \pm \theta_1$  is given by

$$\epsilon = \frac{N(\pi/2 + \theta_1)_{\uparrow} \cdot N(\pi/2 - \theta_1)_{\downarrow}}{N(\pi/2 - \theta_1)_{\uparrow} \cdot N(\pi/2 + \theta_1)_{\downarrow}} - 1. \quad (2)$$

TABLE 2

Results from the transient field measurement

| $v/c$ | $\epsilon$<br>(%) | $\Delta\theta$<br>(mrad) | $\Delta\theta/g$<br>(mrad) | LW<br>(mrad)      | ALW<br>(mrad)     |
|-------|-------------------|--------------------------|----------------------------|-------------------|-------------------|
| 0.015 | $1.8 \pm 0.5$     | $1.2 \pm 0.3$            | $3.6 \pm 0.9$              | 2.7               | 3.9               |
| 0.049 | $10 \pm 2$        | $6.4 \pm 1.4$            | $20 \pm 4$                 | 0.5 <sup>a)</sup> | 0.5 <sup>a)</sup> |

a) See text.

Table 2 summarizes the results of the analysis. The measured effects are corrected for beam bending. The results are also given in rotation angles  $\Delta\theta$  and in rotation per unit g-factor  $\Delta\theta/g$ , calculated with the measured value of the g-factor, see subsect. 3.1. For comparison the rotations  $\Delta\theta/g$  computed from the LW theory and from the ALW model [see refs. <sup>3,4)</sup>] are also listed.

Before discussing these results the possibility of a contribution from the static hyperfine field of Ne in Fe is evaluated. The slowing-down time of <sup>22</sup>Ne ions in Fe (0.7 ps) for the low-velocity measurement is short compared to the nuclear mean life ( $\tau = 5.0$  ps) of <sup>22</sup>Ne( $2_1^+$ ) so that the excited nuclei will experience a static field during some 4 ps. From systematics on measured fields for various nuclei in Fe <sup>16)</sup> one estimates the field on Ne to be of the order of 100 T. From recent time-differential measurements <sup>17)</sup> on <sup>19</sup>Ne in Ni, however, one has some evidence that only 30 % of the implanted Ne-ions experiences this strong field. These estimates lead to a static

field contribution of  $\Delta\theta/g = 1.6$  mrad.

For the high-velocity measurement the thickness of the Fe foil was chosen such that the recoils stopped outside the Fe in the Ag layer so that the static field cannot contribute to the rotation. The  $^{22}\text{Ne}$  ions leave the Fe with an energy of 1.3 MeV as calculated from kinematics and stopping power <sup>12)</sup>. Most of the LW transient field precession, occurring mainly at low energy, is thereby lost and this loss corresponds to  $\Delta\theta/g = 2.6$  mrad.

The rotation observed at high velocity clearly shows a large deviation from the LW value (a factor of 40). In this case the LW and ALW values are identical since the ions do not slow down to further than  $v = v_p$  (see subsect. 2.2). At low velocity the result does not disagree with the LW theory. It may be noted here that since the  $^{22}\text{Ne}(2_1^+)$  mean life is rather long the transient field is probed over the full range from initial to zero velocity. It is therefore not surprising that the low-velocity point is below the ALW value since it was found <sup>10)</sup> for  $^{28}\text{Si}(2_1^+)$  with  $\tau = 0.7$  ps that the measured transient field decreases faster than predicted by the ALW theory between  $v/c = 0.015$  and  $0.006$ .

A probable explanation of the increased transient field at high recoil velocity has been given by Eberhardt et al. <sup>10)</sup>.

In this model the increased field is caused by unpaired polarized s electrons of the moving ion. At high velocities many vacancies exist in inner s shells. Due to fast electron exchange processes between the moving ion and its ferromagnetic surroundings only singly-occupied shells carry the polarization  $\zeta$  of the electrons in Fe. This polarization is taken as  $\zeta = 0.13$  because the exchange with the strongly bound

K and L electrons in Fe is negligible.

To explain the enhanced rotation for  $^{22}\text{Ne}$  at  $v/c = 0.049$  one needs an effective precession time of  $180 \pm 40$  fs in the field of polarized 1s electrons. If it is assumed that the velocity at which the cross sections for loss and capture of 1s electrons are equal is lower than the initial velocity <sup>10)</sup> one obtains an effective time of 100 - 200 fs.

#### 4. Theoretical discussion of the g-factor

Theoretical calculations of the g-factor of the first-excited state of  $^{22}\text{Ne}$  are compared with the experimental value in table 3.

TABLE 3

Comparison of theoretical g-factors with experiment

|                              | g-factor           |
|------------------------------|--------------------|
| Experiment                   | $+0.325 \pm 0.017$ |
| PHF <sup>a)</sup>            | +0.305             |
| Shell-model calculations     |                    |
| Full space: PW <sup>b)</sup> | +0.34              |
| CW <sup>c)</sup>             | +0.38              |
| Truncated: Kuo <sup>d)</sup> | +0.35              |
| PW <sup>d)</sup>             | +0.34              |
| MSDI <sup>d)</sup>           | +0.30              |

a) Ref. 18). b) Ref. 20). c) Ref. 21). d) Ref. 19).

The projected Hartree-Fock <sup>18)</sup> (PHF) as well as the shell-model calculations <sup>19)</sup> with Kuo matrix elements, with Freedom-Wildenthal <sup>19,20)</sup> (PW) matrix elements, which are empirically modified Kuo elements for the  $A = 18-22$  mass region, and with the modified surface-delta interaction (MSDI) do not differ by more than 1.5 standard deviations from the experimental value.

The most recent full sd-space calculation has been performed by Chung and Wildenthal <sup>21)</sup> (CW). They have used Kuo matrix elements, which are modified by a supposedly improved method of fitting energies in the  $A = 18-24$  mass region. Their results obtained for most data are indeed superior to previous calculations. It is therefore surprising that it is just their value that disagrees most with the experimental value.

## 5. Conclusions

In an earlier paper <sup>1)</sup> it has been shown that g-factors can be measured with good precision (5-8 % errors) with the time-differential recoil-into-vacuum method if the fraction of single-electron ions leaving the target foil is only 10-20 %. The present paper shows that even for a single-electron fraction of  $(8 \pm 3)$  % such measurements are possible. Again, as was also found for  $^{20}\text{Ne}$  and  $^{24}\text{Mg}$  <sup>1)</sup>, a large fraction of  $(25 \pm 3)$  % of metastable excited two-electron ions causing a perturbation was observed for two of the targets. This corresponds to 45 % of the total of two-electron ions produced according to the charge fractions given in ref. <sup>13)</sup>. For a carbon-contaminated target a not significant excited two-electron fraction was found and a much

higher ground state one-electron fraction.

It has also been shown that inverse reactions on He-implanted targets are well suited for time-differential experiments since a high recoil velocity is combined with a large observable  $\gamma$ -ray anisotropy in contrast with heavy-ion reactions on heavier targets, see ref. <sup>1)</sup>. The inverse reaction can also be used for a quick determination of the sign of the g-factor with the transient field method at high velocity where the fields are extremely large and hence yield a large experimental effect.

These large experimental effects afford the possibility of transient field g-factor measurements on extremely short-lived states. If very thin Fe foils are used such that the recoil ions spend about 100 fs inside the Fe foil one can use the calibration of the high-velocity transient field by means of a long-lived ( $> 2$  ps) state with a well-known g-factor. This calibration must then also be measured with a thin Fe foil. This procedure does not require the knowledge of the velocity dependence of the transient field.

## References

- 1) R.E. Horstman *et al.*, Nucl. Phys. A248 (1975) 291
- 2) J.F.A. van Hienen and P.W.M. Glaudemans, Phys. Lett. 42B (1972) 301 and private communication
- 3) J.L. Eberhardt, R.E. Horstman, F.V. Heeman and G. van Middelkoop, Nucl. Phys. A229 (1974) 162
- 4) J.L. Eberhardt, R.E. Horstman, H.A. Doubt and G. van Middelkoop, Nucl. Phys. A244 (1975) 1
- 5) W.L. Randolph *et al.*, Phys. Lett. 44E (1973) 36
- 6) G.K. Hubler, H.W. Kugel and D.E. Murnick, Phys. Rev. C9 (1974) 1954
- 7) M. Forterre *et al.*, Phys. Rev. C11 (1975) 1976
- 8) M. Forterre *et al.*, Phys. Lett. 55B (1975) 59;  
J.F.A. van Hienen (Utrecht University), Ph.D. thesis (1975)
- 9) M.B. Goldberg *et al.*, submitted to Phys. Rev. Lett.
- 10) J.L. Eberhardt, G. van Middelkoop, R.E. Horstman and H.A. Doubt, Phys. Lett. 56B (1975) 329;  
J.L. Eberhardt (Utrecht University), Ph.D. thesis (1975)
- 11) J. Lindhard and A. Winther, Nucl. Phys. A166 (1971) 413
- 12) L.C. Northcliffe and K.F. Schilling, Nucl. Data Tables 7 (1970) 233
- 13) J.B. Marion and F.C. Young, Nuclear reaction analysis (North-Holland, Amsterdam, 1968)
- 14) P.M. Endt and C. van der Leun, Nucl. Phys. A214 (1973) 1
- 15) H.D. Betz, Rev. Mod. Phys. 44 (1972) 465
- 16) G.N. Rao, Systematics of dilute impurity hyperfine fields (reported at Int. meeting on hyperfine interactions, Leuven, 1975)
- 17) H. de Waard (Groningen University), private communication
- 18) M.R. Gunye, Phys. Lett. 37B (1971) 125
- 19) J. Koops (Utrecht University), private communication
- 20) B.M. Freedom and B.H. Wildenthal, Phys. Rev. C6 (1972) 1633
- 21) W. Chung and B.H. Wildenthal (Michigan State University), private communication

## CHAPTER III

### CONCLUSIONS

#### 1. The results obtained from the present experiments

The magnetic moments (g-factors) of the first-excited  $I^{\pi}=2^{+}$  states of  $^{20}\text{Ne}$ ,  $^{22}\text{Ne}$  and  $^{24}\text{Mg}$  have been accurately determined with the time-differential recoil-into-vacuum method. The uncertainties in the measured g-factors (4 - 8 %) mainly arose from the fact that fractions of hydrogen-like Ne and Mg ions, produced on recoil into vacuum at velocities of 5 - 6 % of the light velocity, were relatively small. To a lesser extent the uncertainties were determined by the precision of the plunger (see chapters 1 and 2).

The relatively low recoil velocities used in these experiments were mainly imposed by the limit of the terminal voltage (7 MV) of the Utrecht tandem Van de Graaff accelerator. As a result helium- and lithium-like ions were found to contribute prolifically to the hyperfine interaction. The dominant contributions stem from the  $^3\text{S}_1$ ,  $^3\text{P}_1$  and  $^3\text{P}_2$  excited two-electron states. For the  $^{20,22}\text{Ne}$  measurements the relative populations of these states were assumed statistically distributed, i.e. proportional to  $2J+1$ . For  $^{24}\text{Mg}$ , however, the data were sufficiently accurate to deduce these populations. The  $^3\text{S}_1$  state was found to be populated  $2.1 \pm 0.5$  times as strongly as given by the statistical distribution.



The values deduced for the magnetic moments in these cases were found to depend very little on the assumptions on statistical or non-statistical populations since the dipole moments are mainly determined by the hyperfine frequency of the ground-state one-electron ions. For lower-velocity experiments, however, the contributions from hydrogen-like ions become negligible so that a violation of the statistical assumption may have considerable consequences; see e.g. ref. <sup>1)</sup>.

Time-integral deorientation measurements with charge-state separation by a magnetic spectrograph (see chapter 1) can serve, once the g-factor is known, as an independent check on the populations of excited ionic states. The populations extracted for <sup>20</sup>Ne show good agreement with those from the plunger data and are more precise. At the same time it was found that the total charge-state fractions of the ions differ significantly from semi-empirical values <sup>2)</sup>. This is probably due to the dependence on the target foil material; see ref. <sup>3)</sup>.

Evidence for such effects was also found in the <sup>22</sup>Ne plunger experiments where a thin (5  $\mu\text{g}/\text{cm}^2$ ) contaminant layer of carbon on the nickel plunger foil drastically changed the populations of the ionic states (see chapter 2). It would be very interesting to further investigate these effects by time-integral measurements with charge-state separation.

From the point of view of nuclear theory magnetic dipole measurements have proven to be very useful. Although shell-model calculations generally reproduce magnetic moments of doubly even T=0 nuclei rather well and little dependence on both the residual two-particle interaction and the configuration space was found, the accurate experimental value for <sup>24</sup>Mg has shown that the inclusion of  $d_{3/2}$  configurations in

the calculations <sup>4)</sup> is necessary. The calculations for doubly even T=1 nuclei generally show much more sensitivity on the interaction or configuration space; see e.g. ref. <sup>5)</sup>. For  $^{22}\text{Ne}(2_1^+)$ , however, this dependence was found to be small. Nevertheless the accurate experimental value has shown that the supposedly best theoretical value, calculated with Chung-Wildenthal matrix elements <sup>6)</sup>, is higher by more than three standard deviations. A similar deviation is observed for  $^{18}\text{O}(2_1^+)$  measured by the Oxford group <sup>7)</sup>.

## 2. Future experiments within the limitations of the method

In this section the possibilities are reviewed for the extension of magnetic moment measurements with the recoil-into-vacuum method to higher-Z nuclei and shorter-lived states. For this purpose it is necessary to discuss in some detail the time-dependent attenuation of the angular distribution of  $\gamma$ -rays emitted by nuclei after a flight time  $t$ . The contribution of hydrogen-like ions to the attenuation is determined by the coefficients

$$G_k(t) = \left[ 1 - \alpha \frac{k(k+1)}{(2I+1)^2} (1 - \cos\omega t) \right] e^{-t/\tau} \quad (1)$$

in the usual Legendre polynomial expansion of the angular distribution, where  $k = 0, 2, 4, \dots$  is the order,  $\omega$  is the hyperfine frequency for the fraction  $\alpha$  of ground-state hydrogen-like ions,  $I$  is the nuclear spin and  $\tau$  is the mean life of the nuclear state.

For high accuracy it is required that  $\alpha > 0.3$ , so that the hyperfine interaction of hydrogen-like ions amply dominates,

and that  $G_2(t)$  varies over at least 5 %. These requirements imply that the nuclear spin must be  $I \geq 4$ . To have the oscillation not damped too fast the lifetime should be  $\tau > 2\pi/\omega$ . For a gyromagnetic ratio of  $g=0.5$  the hyperfine frequency as a function of atomic number  $Z$  is given by

$$\omega = 0.4(2I+1)Z^3 \times 10^9 \text{ rad.s}^{-1}, \quad (2)$$

so that the mean life must be

$$\tau > 16(2I+1)^{-1}Z^{-3} \times 10^{-9} \text{ s.} \quad (3)$$

For a good determination of the frequency  $\omega$  one needs at least ten measuring points per full period, which corresponds to a distance of  $10 \mu\text{m}$  for a plunger resolution of  $1 \mu\text{m}$ . The ion velocity should satisfy

$$v/c > 6Z \times 10^{-3} \quad (4)$$

in order to have  $\alpha > 0.3$  [see ref.<sup>8)</sup>], which corresponds to an ion energy of  $E > 33 Z^3 \text{ keV}$ . From these arguments it follows that one should have

$$\omega < Z \times 10^{12} \text{ rad.s}^{-1}. \quad (5)$$

Provided that one can produce ions of sufficient energy, magnetic moments of nuclei with atomic number to  $Z_{\text{max}}$  can be measured, where

$$Z_{\text{max}} = 50 / \sqrt{2I+1} \quad (6)$$

as follows from eqs. (2) and (5). Table 1 gives some typical examples of recoil velocities, lifetimes and bombarding ener-

gies for inverse (p,p') and ( $\alpha$ ,p) reactions. This demonstrates the need for beams of high-energetic ions for a large variety of isotopes.

TABLE I

Some properties required for time-differential measurements with inverse reactions on H and He targets <sup>a)</sup>

| Final nucleus |     |                         |        | Bombarding energy $E_{lab}$ ; $E_{cm}$ (MeV) |                |
|---------------|-----|-------------------------|--------|--|----------------|
| Z             | v/c | $\omega$                | $\tau$ | (p,p')                                       | ( $\alpha$ ,p) |
|               | (%) | (rad.ps <sup>-1</sup> ) | (ps)   |  |                |
| 10            | 6   | 2                       | 3      | 40 ; 2                                       | 60 ; 10        |
| 16            | 10  | 8                       | 0.7    | 180 ; 5                                      | 210 ; 20       |
| 20            | 12  | 16                      | 0.4    | 320 ; 7                                      | 350 ; 30       |

a) The numbers for v/c,  $\tau$  and E are lower limits calculated for the first-excited  $I^\pi=2^+$  states of the final nuclei <sup>22</sup>Ne, <sup>34</sup>S and <sup>42</sup>Ca. The protons are detected at 0°.

### 3. Extension to very short lived states

For states with mean lives shorter than given by eq.(3) one can determine g-factors from time-integral measurements on recoil into vacuum provided that the populations of the ionic states are known. These populations should be determined under identical experimental conditions from a time-differential measurement on a longer-lived state of the same nu-

cleus or of another isotope of this nucleus. The time-integral attenuation from ground-state hydrogen-like ions is given by the coefficients

$$G_k(\infty) = 1 - \alpha \frac{k(k+1)}{(2I+1)^2} \frac{\omega^2 \tau^2}{1 + \omega^2 \tau^2} \quad (7)$$

To obtain accurate values for  $\omega\tau$  the population should be  $\alpha > 0.3$  and  $\omega\tau$  should be of the order of unity, hence  $\tau$  should be of the order of

$$\tau = 2.5(2I+1)^{-1} Z^{-3} \times 10^{-9} \text{ s}, \quad (8)$$

which is a factor of six shorter than the lower limit from eq.(3).

Magnetic moments of very short lived states can also be measured with transient magnetic fields at high velocity provided that these fields are calibrated (see chapter 2).

#### References

- 1) F. Beck *et al.*, Proc. Int. Conf. on Hyperfine interactions (Uppland Graviska, Uppsala, 1974), p. 96
- 2) J.B. Marion and F.C. Young, Nuclear reaction analysis (North Holland, Amsterdam 1968)
- 3) H.D. Betz, Revs. Mod. Phys. 44 (1972) 465
- 4) J.E. Koops (Utrecht University), private communication
- 5) J.L. Eberhardt, R.E. Horstman, H.A. Doubt and G. van Middelhoop, Nucl. Phys. A244 (1975) 1
- 6) W. Chung and B.H. Wildenthal (Michigan State University), private communication
- 7) J. Asher *et al.*, J. of Phys. G, to be published

## SAMENVATTING

Theoretische kernmodellen kunnen getoetst worden door de met deze modellen berekende eigenschappen van kernen te vergelijken met experimenteel bepaalde waarden. Om te onderzoeken hoe goed een bepaalde (aangeslagen) toestand in een kern door zo'n kernmodel beschreven wordt, dienen bij voorkeur grootheden gemeten te worden die alleen voor deze toestand karakteristiek zijn, zoals bijvoorbeeld het magnetische dipool- of het elektrische quadrupoolmoment.

In dit proefschrift wordt beschreven op welke wijze de magnetische dipoolmomenten van de eerste aangeslagen toestanden in  $^{20}\text{Ne}$ ,  $^{22}\text{Ne}$  en  $^{24}\text{Mg}$  nauwkeurig werden gemeten. Deze toestanden hebben gemiddelde levensduren tussen 1 en 5 ps. In het kort komt de meetmethode op het volgende neer.

Met kernreacties, waarbij zware ionen met hoge energie op een dun trefplaatje worden geschoten, worden kernen in een aangeslagen toestand geproduceerd, die met grote snelheid door het trefplaatje heen het vacuum in vliegen. Bij een juiste keuze van de snelheid (zie hoofdstuk 3) verlaat een grote fractie van de aangeslagen kernen het folie vergezeld van slechts één electron in de 1s baan. Ten gevolge van de hyperfijne wisselwerking in een zo ontstaan waterstofachtig ion zullen het electron met spin  $\vec{J}$  en de kern met spin  $\vec{I}$  gaan precederen om het totale impulsmoment  $\vec{F} = \vec{I} + \vec{J}$ , waarbij  $F$  in dit geval de waarden  $I \pm \frac{1}{2}$  kan aannemen. De interferentie die nu optreedt tussen de toestanden met hyperfijne energieën  $E_{I+\frac{1}{2}}$  en  $E_{I-\frac{1}{2}}$  wordt waargenomen als een oscillatie in de onder een zekere hoek gemeten intensiteit van de bij het verval van de kern uitgezonden  $\gamma$ -straling. De hyperfijne wisselwerking wordt,

door de ionen op te vangen in een metalen plaatje op een variabele afstand van het trefplaatje, uitgeschakeld ten gevolge van electronenvangst.

De afstand tussen de beide plaatjes fungeert nu als een klok (in het ps gebied!) waarmee de oscillatie tijd-differentieel gemeten wordt. Het magnetische dipoolmoment is evenredig met de frequentie van deze oscillatie.

In hoofdstuk 1 worden metingen beschreven aan de laagste aangeslagen toestanden van de kernen  $^{24}\text{Mg}$  en  $^{20}\text{Ne}$ . Tegelijkertijd werd de levensduur van deze toestand in  $^{24}\text{Mg}$  (2,1 ps) nauwkeurig bepaald. Onder de ionen die uit het trefplaatje vliegen is ook een grote fractie helium-achtige ionen aanwezig. Uit de tijd-differentiële metingen, aangevuld met metingen waarbij de ionen naar lading werden geselecteerd met behulp van een magnetische spectrograaf, werd voor  $^{20}\text{Ne}$  vastgesteld dat 60 % van deze helium-achtige ionen zich bevindt in aangeslagen toestanden met een sterke hyperfijne wisselwerking.

De meting van het magnetische moment van de eerste aangeslagen toestand in  $^{22}\text{Ne}$  en de mogelijkheid om met deze waarde de grootte van het magneetveld te bepalen, dat optreedt tijdens het afremmen van Ne in gemagnetiseerd ijzer, worden beschreven in hoofdstuk 2.

In de hoofdstukken 1 en 2 worden bovendien de door verschillende theorieën voorspelde magnetische dipoolmomenten vergeleken met de experimenteel bepaalde.

In hoofdstuk 3 worden de behaalde resultaten besproken en de mogelijkheden aangegeven om de metingen binnen de grenzen van de methode uit te breiden naar korter levende toestanden in kernen met een hoger atoomnummer.

## CURRICULUM VITAE

De schrijver van dit proefschrift werd in 1948 te Schiedam geboren. In 1966 begon hij, na het behalen van het diploma gymnasium 8 aan het "Amersfoorts Lyceum", zijn studie in de wis- en natuurkunde aan de Rijksuniversiteit te Utrecht. Na het behalen van het kandidaats examen in 1969 met als hoofdvakken natuur- en scheikunde en als bijvak wiskunde, werd in 1971 het doctoraal examen natuurkunde met als groot bijvak scheikunde behaald. Sindsdien is hij werkzaam in de Utrechtse werkgroep kernfysica als wetenschappelijke medewerker van de Stichting voor Fundamenteel Onderzoek der Materie. Naast zijn onderzoek gaf hij werkcolleges natuurkunde aan voor-candidaats studenten in de natuurkunde en assisteerde hij op natuurkunde practica van studenten in de chemie, farmacie en biologie.

---

